DEVELOPMENT OF A PROTOTYPE NORTH PACIFIC OCEAN SURFACE VISIBILITY CLIMATOLOGY STRATIFIED BY OBSERVATION TIMES

Thomas Norman Talbot

NPS 63-81-002

NAVAL POSTGRADUATE SCHOOL
Monterey, California

THESIS

DEVELOPMENT OF A PROTOTYPE NORTH PACIFIC OCEAN SURFACE VISIBILITY CLIMATOLOGY STRATIFIED BY OBSERVATION TIMES

by

Thomas Norman Talbot

June 1981

Thesis Advisor: R. J. Renard

Approved for public release; distribution unlimited.

Prepared for: Naval Air Systems Command
Washington, D.C. 20360

NAVAL POSTGRADUATE SCHOOL
Monterey, California

Rear Admiral J. J. Ekelund
Superintendent

David A. Schrady
Provost

This thesis prepared in conjunction with research supported by the Naval Air Systems Command (AIR 370).

Reproduction of all or part of this report is authorized.

Released as a
Technical Report by

REPORT DOCUMENTATION PAGE	READ INSTRUCTIONS BEFORE COMPLETING FORM
1. REPORT NUMBER NPS 63-81-002	2. GOVT ACCESSION NO.
	3. RECIPIENT'S CATALOG NUMBER
4. TITLE (and Subtitle) Development of a Prototype North Pacific Ocean Surface Visibility Climatology Stratified by Observation Times	5. TYPE OF REPORT & PERIOD COVERED Master's Thesis; June 1981
	6. PERFORMING ORG. REPORT NUMBER
7. AUTHOR(s) Thomas Norman Talbot and Robert J. Renard	8. CONTRACT OR GRANT NUMBER(s)
9. PERFORMING ORGANIZATION NAME AND ADDRESS Naval Postgraduate School Monterey, California 93940	10. PROGRAM ELEMENT, PROJECT, TASK AREA & WORK UNIT NUMBERS para 1D 62759N: WF59-551 N6685681NR81003
11. CONTROLLING OFFICE NAME AND ADDRESS Naval Postgraduate School Monterey, California 93940	12. REPORT DATE June 1981
	13. NUMBER OF PAGES 85
14. MONITORING AGENCY NAME & ADDRESS(if different from Controlling Office)	15. SECURITY CLASS. (of this report) Unclassified
	15a. DECLASSIFICATION/DOWNGRADING SCHEDULE

16. DISTRIBUTION STATEMENT (of this Report)

Approved for public release; distribution unlimited.

17. DISTRIBUTION STATEMENT (of the abstract entered in Block 20, if different from Report)

18. SUPPLEMENTARY NOTES

19. KEY WORDS (Continue on reverse side if necessary and identify by block number)

North Pacific Ocean Visibility
Visibility
Marine Visibility
Marine Fog

20. ABSTRACT (Continue on reverse side if necessary and identify by block number)

This study develops a prototype surface visibility climatology for the North Pacific Ocean. Data provided by the Naval Oceanographic Command Detachment, Asheville, North Carolina, were extracted from the National Climatic Center's historic files and represent a 20-year (1954-1973) period. The area of study is bounded by latitudes 20°N and 70°N and longitudes 120°E and 110°W. Experiments concerning the

implementation and modification of an objective processing and analysis routine are briefly described. Select Greenwich Mean Time and Local Standard Time (LST) visibility analyses and their standard deviations for January, April, July and October are developed from a data base of nearly 1.6 million transient ship observations. Each set is analyzed for the diurnal variation of visibility at sea. The LST analyses are found to be unacceptable for use in the investigation of diurnal visibility changes due to an intermediate synoptic time low-visibility bias. Marine fog frequencies from a 10-year period (1967-1976) are shown; they compare favorably with the visibility analyses for comparable time periods.

Development of a Prototype North Pacific Ocean Surface Visibility Climatology Stratified by Observation Times

by

Thomas Norman Talbot
Captain, United States Air Force
B.A., University of Vermont, 1972

Submitted in partial fulfillment of the
requirements for the degree of

MASTER OF SCIENCE IN METEOROLOGY

from the

NAVAL POSTGRADUATE SCHOOL
June 1981

ABSTRACT

This study develops a prototype surface visibility climatology for the North Pacific Ocean. Data, provided by the Naval Oceanographic Command Detachment, Asheville, North Carolina, were extracted from the National Climatic Center's historic files and represent a 20-year (1954-1973) period. The area of study is bounded by latitudes 20° N and 70° N and longitudes 120° E and 110° W. Experiments concerning the implementation and modification of an objective processing and analysis routine are briefly described. Select Greenwich Mean Time and Local Standard Time (LST) visibility analyses and their standard deviations for January, April, July and October are developed from a data base of nearly 1.6 million transient ship observations. Each set is analyzed for the diurnal variation of visibility at sea. The LST analyses are found to be unacceptable for use in the investigation of diurnal visibility changes due to an intermediate synoptic time low-visibility bias. Marine fog frequencies from a 10-year period (1967-1976) are shown; they compare favorably with the visibility analyses for comparable time periods.

TABLE OF CONTENTS

LIST OF TABLES

LIST OF FIGURES

ACKNOWLEDGMENTS

My sincere appreciation is extended to my thesis advisor, Dr. Robert J. Renard, whose constant interest, guidance and thoughtful suggestions made this research both a challenging and positive experience. I also extend my gratitude to Dr. Kenneth L. Davidson for his review of the manuscript. Thanks also go to Mr. William J. Thompson for his generous assistance with the computer processing aspects of the study, especially his creative assistance in overcoming numerous computer problems at the beginning of the research.

I also thank Mr. Michael McDermet and his staff for their technical assistance and suggestions, particularly in getting the analyses into a final form.

I am also indebted to the staff at the W. R. Church Computer Center for the effective, professional assistance which I received throughout this project.

Final thanks go to my fellow graduate students, whose friendship, interest and timely encouragement made the occasional difficult periods pass quickly.

I. INTRODUCTION AND BACKGROUND

Visibility is an important meteorological parameter which has a significant impact upon maritime operations. Ship routing, transit times and aircraft operations are but a few of the operational areas highly affected by visibility. Wheeler and Leipper (1974) investigated the impact of visibility restrictions due to fog on United States Naval Operations from both historical and modern perspectives. One of their conclusions is that increasing the probability of mission success and minimizing the probability of failure may well be related to accurate forecasting of visibility restrictions due to fog. Effective mission planning must include visibility considerations, as failure to do so may seriously jeopardize mission success.

Certain inherent difficulties have existed in the formulation of marine visibility climatologies. The vast size of the oceans presents a problem as no organized fixed weather observation reporting system exists except for a small number of Ocean-Weather-Stations (OWS) scattered around the world. As a result, observations have been typically taken by merchant ships, trawlers, military vessels and other transiting ships. The fact that many of these ships do not have a trained weather observer makes the

validity of the observations often questionable. Other observing difficulties are that ships are usually in motion when observations are taken, further adding to the difficulty of recording accurate observations, and that unlike on land, fixed points of reference are usually absent while a vessel is at sea, making accurate visibility observations difficult. Other problems can be related to the density of observations at sea. Many ship observations are often limited to the main shipping routes and coastal regions. This situation results in a dense network of observations existing in these regions, with comparatively sparse data existing elsewhere. Additionally, attempts by ships to avoid areas of unfavorable weather may contribute toward a fair weather bias (Quayle, 1974).

In view of the above discussion, a continuing need exists for accurate and representative visibility climatologies. Research in recent and past years at the Naval Postgraduate School (NPS) has sought to improve surface visibility forecasting for the North Pacific Ocean (Schramm, 1966; Nelson, 1972; Aldinger, 1979; Selsor, 1980; Yavorsky and Renard, 1980). In spite of the successive increases in skill shown by these studies, few operationally determined forecast products are currently available to inform a ship of impending restrictions in visibility. Thus, planning and operational decisions may continue to be highly dependent upon the use of a marine visibility climatology, at least until improved forecasting techniques become operationally available.

II. OBJECTIVES

The primary objective of this study was to develop a surface visibility climatology for the North Pacific Ocean. The development of the climatology includes experiments with an objective analysis routine to produce meteorologically sound analyses.

Secondary objectives include applying the analysis procedures developed for the visibility data to a set of data representing fog frequencies in the study area. The developed frequency climatology is compared to the visibility climatology for use as an aid in the interpretation of the visibility climatology. Another secondary objective includes the study of diurnal variations in visibility over the North Pacific Ocean.

The following represent minimum requirements for the visibility climatology:

A. Analysis of the density of ship observations
B. Analysis and interpretation of mean surface visibilities
C. Analysis and interpretation of surface visibility standard deviations
D. Categorical display of visibility frequencies
E. Development of visibility analyses at local standard times
F. Analysis of fog frequencies

III. PROCEDURES AND EXPERIMENTS

A. DATA

The data for this study consist of 20 years (1954-1973) of transient ship surface visibility observations for the North Pacific Ocean. Data, provided by the Naval Oceanography Command Detachment, Asheville, North Carolina, were extracted from the National Climatic Center's historical files and are on magnetic tape in a Marsden square-subsquare-month-hour format. Figure 1 shows the global network of 10° latitude X 10° longitude Marsden squares. Each Marsden square consists of 100 subsquares (1° lat X 1° long). Data exist for all months of the year and include both primary (0000, 0600, 1200, 1800 GMT) and secondary (0300, 0900, 1500, 2100 GMT) synoptic times, numbering approximately 4.5 million individual observations. Table I presents a breakdown of the observations by synoptic times.

B. AREA

The area of study selected is the North Pacific Ocean between 20° N and 70° N lat from 120° E to 110° W long (Figure 2). The grid points of this projection correspond to Fleet Numerical Oceanography Center's (FNOC) 63X63 gross mesh grid with a mesh size of 381 km at 60° N lat. This area includes those regions recently used for statistical

studies of marine fog at NPS (Englebretson, 1974; Willms, 1975; Aldinger, 1979; Koziara, 1980; Yavorsky and Renard, 1980; Selsor, 1980).

C. INITIAL PROCESSING OF DATA

A total of 56 Marsden squares are wholly or partially contained within the grid study area. The initial formatting of the data by the National Climatic Center made the task of searching for erroneous data unnecessary. The month of July was chosen for the initial analyses and experiments. This choice was made because July is the month with the lowest average surface horizontal visibility as well as the month exhibiting stable circulation patterns.

D. OBJECTIVE ANALYSIS ROUTINE

The objective analysis routine used here is the circular scan type devised by Cressman (1959). The routine applies a series of corrections to a first-guess field. The corrections are based on the input of data available in the vicinity of each grid point. In the routine, the amount of weight (W) or influence that a given observation has on the grid point value is given by the relation $W = (R^2 - D^2)/(R^2 + D^2)$ where R is the scan radius and D is the distance from the grid point to the observation. The grid point is then corrected by using successively smaller scans about the grid point to search for data.

For all visibility analyses, both land and over-ocean grid points were initialized with the mean value of the field. Attempts at achieving a more precise initialization were not pursued because of the fairly uniform data density of the fields. Naturally, using an average initialization resulted in the data-exempt regions being assigned the mean value in the final analysis. For all ship density analyses, all grid points located over the land were initialized to zero (i.e., no ships over land) while the remaining over-water grid points were assigned the average value of the field. This scheme permitted a better depiction of coastal shipping routes than would be achieved otherwise.

E. SELECTION OF A GRID SIZE

Initially the study area consisted of a 32 X 16 grid point array, with the mesh size or distance between grid points (at 60° N lat) equal to 381 km per grid point interval. In an effort to achieve more detail in the analyses, a one-half mesh grid size, equating to 190.5 km at 60° N lat, and a one-third mesh grid size, equating to 127 km at 60° N lat, were produced. These grids equate to arrays containing 63 X 31 and 94 X 43 grid points, respectively. Analyses produced with all three mesh sizes were compared utilizing a wide variety of scanning radii. Scanning radii determine how far from each grid point data are selected to correct the grid-point value. A scanning radius of "1"

represents a data scan of one mesh length from a given grid point. Scanning radii used in combination with the three mesh sizes included 1, 7/8, 3/4, 7/10, 1/2, 3/8 and 1/4. A comparison of the three mesh sizes indicated that the full mesh size was too large for the study. Data appeared to be excessively smoothed and lacked detail. This smoothing sharply contrasted with the one-third mesh analysis which produced excessive detail in some areas and gave a cluttered appearance. The one-half mesh grid size with three successive scans and a scanning radius of 7/10 became a suitable compromise in that it produced considerable detail while still permitting the analysis to appear meteorologically sound.

F. ANALYSIS PROCEDURES

1. Greenwich Mean Time Analyses

With the successful implementation of an analysis scheme on July data, only minor changes were made to permit the systematic production of analyzed charts for the remaining months. All computations were processed using the IBM System 370 digital computer at the NPS Computer Facility. The analyzed meteorological fields were plotted using a system routine named CONTUR, which uses a VERSATEC plotter. Although individual isoline values are assigned by the computer, individual maxima and minima appearing on figures of

the visibility analyses represent 5° X 5° averages and individual maxima appearing on the data density analyses represent the maximum number of observations per Marsden subsquare. Additionally, portions of the grid-area extending beyond the 20° N lat southern data boundary (southeast and southwest corners) were left blank. Further editing was required along the geographical boundaries which were often regions of strong gradients. Whenever possible, the actual 'raw' data were considered in determining the most representative coastal gradients. Because of the editing, the boundary portions of the analyses are not as representative of the actual surface visibilities as are the unedited, central portions of the study area.

2. Local Standard Time Analyses

Producing a Local Standard Time (LST) analysis required a combination of three GMT data fields. Since data exist every three hours, starting at 0000 GMT, it was also possible to produce LST analyses in three-hour intervals. To illustrate the process used, consider the following example describing a 0000 LST analysis. The 0000 hour (accurate to within one hour) local analysis represents a combination of 1500 GMT data from the geographical area of 120° E to 157.5° E long, 1200 GMT data from the region of 157.5° E to 157.5° W long, and 0900 GMT data from 157.5° W to 110° W long. In all analyses produced, it is apparent that the

region consisting of 0900 GMT data (157.5° W to 110° W long) is inconsistent with the remainder of the analysis, thereby negating any type of meaningful interpretation. To compensate for the deficiencies of the secondary synoptic time, analyses were produced which utilized a blend of two synoptic times. In the region from 120° E to 157.5° E long, a 0130 LST analysis consists of a combination of 1500 GMT and 1800 GMT data sets. The 0130 local-time represents a three-hour window which is accurate to within 1.5 hours. If data from either synoptic time exist in a given Marsden subsquare, they are incorporated in the analysis. If data exist from each synoptic time in a given Marsden subsquare, a simple average of the mean visibilities is used. A weighted combination was not used so as not to overly bias the data to the data dense, primary synoptic time values. Data were similarly combined in the other two regions of the study area. This procedure has the desired effect of presenting an aesthetically pleasing analysis.

3. Fog Frequency Climatology

To further assist in the interpretation of the visibility analyses, it was determined to produce a series of climatological fog frequencies. The original data set was also provided by the Naval Oceanography Command Detachment, Asheville, North Carolina and represents a 10-year (1967-1976) sample of data. Analysis techniques developed for the visibility data were applied to the fog data. The

analyses produced represent the frequency of occurrence (%) of fog in any form at all times for a given month.

4. Latitudinal and Longitudinal Band Averaging

Investigation into the possible diurnal variation in surface visibility for July involved longitudinal and latitudinal band averaging. The band averaging technique allows specific regions, such as an area of known low visibility, to be investigated free from the influence of the remainder of the study area. This regional approach assists in the interpretation of the local-time analyses. Table II presents a weighted mean surface visibility[1] for all synoptic times for the entire area and for portions of the study area on either side of the 180° meridian. A bias evident for each area is that all intermediate GMT-time means are lower than those of the adjacent primary GMT times. Tables III and IV show band averaged local standard time (LST) mean visibilities along with those of the two GMT times contributing to each LST. The GMT bias has the effect of inducing a similar bias in the LST values. Prior fog studies (Englebretson, 1974; Renard, 1976) do not reveal a corresponding bias in primary versus intermediate time values. Figure 3 represents a 12-year (1963-1974) sample of diurnal fog frequencies for stationary Ocean-Weather-Station Papa (50° N lat, 145° W long) in the North Pacific

---

[1] Weighting is according to number of observations in each Marsden subsquare.

Ocean; no oscillation of the type noted in this study is apparent. Additionally, personnel at the National Climatic Center, Fleet Numerical Oceanographic Center, ocean routing specialists, NPS Meteorology staff members and fellow graduate students were consulted in an effort to explain the bias. The inquiries led to a wide variety of possible explanations. The most likely explanation suggests that ships at sea take and transmit weather observations at the primary synoptic times and that intermediate-time observations are most likely taken only when the ship is experiencing significant weather such as high winds, high seas, heavy precipitation or similar such events. In general, these events would be associated with relatively low visibility. Table V provides statistical support for this explanation. The area from 50° to 60° N lat, 120°E to 180° long represents a region of poor visibility. In this region, intermediate observations comprise 34% of all observations. However, in the higher visibility region of 20 to 30 N lat, intermediate observations represent only 22% of all observations.

World Meteorological Organization Technical regulations (1979) No. A.1.2-3.1.5 provides support for this explanation:

> "Whenever storm conditions threaten or prevail, surface synoptic observations should be made

> and reported from a mobile ship more frequently
> than at the main standard times."

"More frequently" is most likely to mean intermediate observation times in addition to primary observation times. The effect of such a "bad-weather" bias in observations is to contaminate the LST analysis with an oscillation due to the relatively low visibilities associated with these intermediate synoptic-time values.

IV. RESULTS

The following discussion considers analyses from the months of July, October, January and April. These represent a small portion of the total analyses produced. In that the most significant visibility restrictions occur in summer, July is the first month discussed. In most cases, analysis interpretation consists of relating the significant aspects of each analysis to regional climatology. Generally, 0000 GMT and 1200 GMT anlayses are used because 0000 GMT represents a daylight period and 1200 GMT a night period over most of the study area. However, additional July 0600 GMT and 1800 GMT analyses are included to permit an investigation into possible diurnal variations in visibility from the primary synoptic time analyses. Primary synoptic times refer to 0000, 0600, 1200 and 1800 GMT whereas secondary or intermediate times refer to 0300, 0900, 1500 and 2100 GMT.

A. JULY

Figures 4a, 4b and 5a represent the 0000, 0900 and 1200 GMT density of transient ship observations in the study area. On the 0000 and 1200 GMT analyses, the cross-oceanic and eastern North Pacific Ocean shipping lanes are apparent with the shipping route from the California coast to the

Hawaiian Islands containing the most concentrated network of observations. Poleward of 45° N lat, the great-circle route across the North Pacific Ocean is evident. Maximum values for any Marsden subsquare (1° lat X 1° long area) occur adjacent to San Diego where 397 and 279 observations are recorded at 0000 and 1200 GMT, respectively. The intermediate time analysis at 0900 GMT is presented as a comparison to the primary-time analyses. The well defined shipping routes of the primary-time analyses are absent because 0900 GMT is an intermediate time and relatively few observations are taken. A comparison of the total observations in each Marsden square for 0000 and 0900 GMT indicates that in 23 of the 56 Marsden squares comprising the study area, primary-time observations exceed intermediates by at least one order of magnitude.

The corresponding surface ship visibilities for 0000, 0900 and 1200 GMT are shown in Figs. 5b, 6a and 6b with the standard deviations for 0000 GMT shown in Fig. 7a. The highest standard deviation values occur in the intermediate zone between the low visibility values northward and high values to the south. The high standard deviation values indicate a much higher variability in visibility values in this region as compared with the more uniform high visibility values to the south. A comparison with lower visibilities

poleward is difficult because the tight gradients may be related to the sparse data existing in these regions.

The 0900 GMT visibility analysis differs significantly from the 0000 and 1200 GMT analyses which have common regions of high and low visibility values and well defined gradients of visibility in which the isolines tend to follow the latitude circles. The 0900 GMT analysis appears chaotic and noisy, with a much higher incidence of local maxima and minima. Initially, the characteristics of the 0900 GMT analysis appeared to be a result of the low density of data at the intermediate time. However, the band averaging experiment provided further insight into the problem. It is apparent that the intermediate times contain more extreme lower visibility values than the primary synoptic times, causing the essential character of these analyses to differ considerably form those of primary synoptic times. Further support for this explanation is evident by comparing the 0900 to the 1200 or to the 0000 GMT analyses. The local minimums of 6, 7 and 8 km on the 0900 GMT analysis are much lower than the 11 and 12 km minimum values of the 0000 and 1200 GMT analyses. In the high visibility areas (lower latitudes) the 0900 GMT values are more representative of that small percentage of time with relatively low visibility.

As Fig. 7b indicates, the dominant summer meteorological feature for the North Pacific Ocean is the Subtropical High

which is centered near 35° N lat, 150° W long with a central pressure of 1025 mb. To the west, low pressure exists with minimum values over the Asian continent. The Asiatic low pressure system interacts with the Subtropical High to produce southerly wind components in the region to the west of 150° W long. Equatorward of 35° N lat these winds have southeastern components and poleward of 35° N lat, southwesterly components. The 35° N lat circle also marks the northern extent of near-homogeneous, tropical surface water. Poleward of 35° N lat, sea-surface temperatures (SST) become increasing colder with latitude. This change in wind component and SST gradients coincide with the northern boundary of high visibility values. Poleward of this region, visibility values show a sharp decrease to near 45° to 50° N lat where minimum values are located. The poleward transport of warm, moisture-laden air by the southwest winds over increasingly cooler ocean water eventually saturates the near-surface air, producing fog. As a result, both the 0000 and 1200 GMT analyses contain low visibility regions poleward of 35° N lat and west of 150° W long. The minimum visibility region in the 0000 GMT analysis is located southeast of the Kamchatka Peninsula near 48° N lat, 155° E long. In this region, the cold Arctic waters transported by the Oyashio Current are overridden by the warm, humid air of the

southwesterlies. The transported air, with a history of considerable fetch over the relatively warm ocean water, readily approaches saturation in this area. It is this combination of events which is most likely responsible for the formation and maintenance of minimum visibilities in this region.

The region east of 150° W long on the eastern periphery of the Subtropical High is a region of persistent conditions where winds tend to have a northerly component. As a result, cooler air is being transported into this region from the temperate latitudes with corresponding improved visibilities. This improvement is evident in both the 0000 and 1200 GMT analyses by the northward intrusion of higher visibility values to the east of 150° W long. The California coastal region is an exception because of the cold surface water present due to upwelling. The temperature contrast between the cold ocean water and the overlying air induces fog formation and visibility restrictions.

All three analyses show that the highest visibilities in the study area exist equatorward of 35° N lat. This is a region where the sea-surface temperatures are uniform and high. High visibilities are correlated with easterly winds over this region which are transporting air from the eastern side of the Subtropical High which is cooler than the underlying sea, making fog formation unlikely.

Figures 8a and 8b show the July 0600 GMT and 1800 GMT mean surface visibilities, respectively. Comparing all four July primary-time mean surface visibilities for diurnal variations in visibility required separating each analysis into three regions. The western North Pacific Ocean region refers to that area from 120° E to 157.5° E long, the central North Pacific Ocean region extends from 157.5° E to 157.5° W long and the remainder of the area extends from 157.5° W to 110° W long. For a specific GMT, each region includes three corresponding local standard times. For the most western region these are as follows:

GMT	Local Standard Time		
0000	0800	0900	1000
0600	1400	1500	1600
1200	2000	2100	2200
1800	0200	0300	0400

As is evident, the 0000 and 0600 GMT analyses represent daylight periods. Comparisons of these two analyses with the 1200 and 1800 GMT analyses, which represent late afternoon and night periods, respectively, indicate that the highest visibilities exist for the daylight period analyses. In the 1200 and 1800 GMT analyses, visibilities are consistently 2-4 km lower than either daylight period analyses. This

lower visibility for the 1200 GMT analysis may result from the late afternoon low angle of sunlight highlighting the atmospheric pollutants and particulates, thus apparently lowering visibility. The 1800 GMT low visibility values may result from a night-time related lowering of visibility.

Corresponding GMT/LST values for the central region are as follows:

GMT	Local Standard Time		
0000	1100	1200	1300
0600	1700	1800	1900
1200	2300	0000	0100
1800	0500	0600	0700

The daylight periods represented by the 0000 and 0600 GMT analyses are similar except for an extension of lower visibilities along 50° N lat in the eastern portion of the 0600 GMT analysis. This low visibility extension may be due to the previously described, late-afternoon related visibility restrictions. Comparing the 0000 GMT (daylight) analysis with the 1200 GMT (night) and 1800 GMT (early morning) analysis in the central North Pacific Ocean region indicates visibilities in both the 1200 and 1800 GMT analyses of 2-4 km lower than in the 0000 GMT analysis. These comparisons indicate better visibilities for daylight periods than for night and dawn periods in this region.

In the eastern region, both GMT and LST are related as follows:

GMT	Local Standard Time		
0000	1400	1500	1600
0600	2000	2100	2200
1200	0200	0300	0400
1800	0800	0900	1000

The 0000 GMT analysis represents a mid-afternoon period and contains higher visibilities than corresponding analyses. The 0600 GMT analysis is generally 1-2 km lower in visibility than the 0000 GMT, again possibly indicating a lowering of visibility due to the peculiarities associated with near-sunset time. The largest variations are present between the 0000 (mid-afternoon) and 1200 GMT (night) analysis. Throughout the region, 0000 GMT visibilities generally exceed those of the 1200 GMT analysis by 3-5 km. These sharp contrasts are modified when the 0000 GMT analysis is compared with the 1800 GMT (mid-morning) analysis. However, 0000 GMT values still exceed those of the 1800 GMT analysis by 1-2 km. It must be noted that the differences in these regions as described above may be due in large part to observer-associated biases.

The next series of analyses discussed are those depicting the frequency of occurrence of certain visibility categories. These categories are for 1) visibility less than

2 km, 2) visibility equal to or greater than 2 km but less than 10 km, and 3) visibility greater than or equal to 10 km. This three-category approach follows Selsor (1980) whose research indicated that these categories represent a suitable categorization of operationally significant parameters. Figures 9a and 9b show frequencies of occurrence less than 2 km for 0000 and 1200 GMT, respectively. These show maximum values south and southeast of the Kamchatka Peninsula and to the west of the Peninsula. These regions are generally consistent with the 0000 and 1200 GMT visibility analyses. One difference between the analyses is the magnitude of the maximum appearing in the Sea of Okhotsk, west of the Kamchatka Peninsula. Since this is a data-sparse region, the differences may be directly related to the number of observations contributing to the analysis. Elsewhere in the study area, the two analyses are very similar.

As with the mean surface visibilities, additional 0600 GMT and 1800 GMT frequencies of visibility less than 2 km were produced to allow further investigation into possible diurnal variations in visibilities. These are shown in Figs. 10a and 10b. The regional scheme of study and the relationship of GMT to LST's are identical to those used in the mean surface visibility discussion. The strongest support for a diurnal variation in the western North Pacific Ocean

region (120° E to 157.5° E long) is present in the comparison between the 0000 GMT (0800 LST, 0900 LST, 1000 LST) and the 1800 GMT (0200 LST, 0300 LST, 0400 LST) analyses. Frequencies of low visibilities are more extensive, especially to the west of the Kamchatka Peninsula for the 1800 GMT analysis. The central North Pacific Ocean region (157.5° E to 157.5° W long) shows little support for diurnal variations. The 1200 GMT (2300 LST, 0000 LST, 0100 LST) analysis and the 1800 GMT (0500 LST, 0600 LST, 0700 LST) contain larger values and more extensive regions of low visibility frequencies than the 0000 GMT (1100 LST, 1200 LST, 1300 LST) or the 0600 GMT (1700 LST, 1800 LST, 1900 LST) analysis. However, the variations are primarily restricted to the 40° N to 50° N lat band. The eastern region also contains little support for diurnal variations in visibility. This can be partially attributed to the absence of low-visibility frequencies in excess of 20% in this region.

Figures 11a and 11b show 0000 and 1200 GMT frequency of occurrence of visibilities equal to or greater than 2 km to values less than 10 km. A comparison of the two analyses indicates that the 0000 GMT analysis has the maximum frequency of 30% approximatley 5 degrees north of the 1200 GMT maximum. The relative data densities may be related to this displacement as 0000 GMT observations exceed those of 1200 GMT by

27% in this region. Also noted is the extension of the 20% isoline in the 1200 GMT analysis from the Kamchatka Peninsula well into the Gulf of Alaska whereas the 0000 GMT 20% isoline is confined to the Bering Sea. Again, this may indicate a diurnal variation with higher frequencies (i.e., lower visibilities) being more extensive during the night period, at least where visibilities are near climatological minimal values.

Figures 12a and 12b represent the 0000 and 1200 GMT frequencies of occurrence of visibility greater than or equal to 10 km. Significant differences again may be diurnally related. The minimum value in the 1200 GMT analysis, while located in the same region as the minimum in the 0000 GMT analysis, is 10% lower in magnitude, indicating poorer visibility. In addition, isolines of lower frequencies (thus poorer visibility) in the 1200 GMT analysis include larger portions of the study area than corresponding isolines of the 0000 GMT analysis.

Figure 13a shows the frequency of observed fog for July, independent of time. This analysis compares very favorably with Figs. 12a and 12b, frequencies of occurrence of visibility greater than or equal to 10 km. As a first approximation, fog frequency (%) equals 100 minus the frequency of visibility greater than or equal to 10 km. Gradients in each analysis also compare favorably with the exception being

the geographical boundaries. Differences here may be a result of the initialized mean over-ocean value present over land areas adjusting to the 'corrected' over-ocean values. The similarities of the visibility and fog frequencies clearly indicate that most of the July visibility restrictions in the North Pacific Ocean are due to fog.

Figures 13b and 14a show 0000 LST and 0130 LST analyses. The 0000 LST analysis was developed for an investigation into possible diurnal variations in visibility at sea. The analysis is not very useful due to the noise which is present to the east of 157.5° W long due primarily to the use of 0900 GMT data in this portion of the analysis. To overcome the intermediate time inconsistency, two different synoptic times (one primary and one intermediate) were combined over the entire region to give the 0130 local hour analysis, accurate to within 1.5 hours. As is apparent, the combination has the desired effect of smoothing the analysis. However, due to the large, apparently non-meteorological, differences in mean visibilities between primary and secondary synoptic times (six-hour wave), it was determined that diurnal variations in visibility at sea, using this approach, would not be valid.

B. OCTOBER

Figures 14b, 15a and 15b show 0000, 0900 and 1200 GMT surface visibility analyses for October. These figures indicate a significant improvement in surface visibilities from July values. Figure 16a shows the 0000 GMT standard deviations. Over the entire study area, the October standard deviations are slightly lower than those of July which indicates less variability. In the region from 40° to 50° N lat, the lower visibility values are located in the region of higher standard deviations. This indicates greater variability in the vicinity of low visibility regions. As in July, low standard deviation values are found in the southern portions of the study area where the highest visibility values (least variable) are found. The extremely tight gradients in the northern portions of the analysis may be related to the sparse data in the region.

The climatology of the North Pacific Ocean in October (Fig. 16b) indicates a weakening of the Subtropical High. Two high pressure cells at 35° N lat, 140° W long and 35° N lat, 175° E long are located along the axis of the Subtropical High which follows the 35° N lat circle. As a precursor of winter, the Aleutian Low appears ($<$ 1000 mb) in the Gulf of Alaska and the Siberian High increases in strength over the Asian continent. The resultant wind regime consists of winds with a northerly component along the California coast

with open-ocean easterly components south of 35° N lat and westerly components poleward of 35° N lat. The predominately zonal nature of the prevailing winds throughout most of the region does not support substantial horizontal heat and moisture transport. This is particularly true when the wind components tend to parallel the SST gradients. This situation results in the ambient air temperature approaching the underlying SST, a situation generally unfavorable for fog formation. Figure 17a, frequency of occurrence of fog in any form, also indicates the low occurrence of fog over the study area, except for the North American coast. As a result, visibility is high, exceeding 15 km throughout the analyses, with correspondingly weak visibility gradients. The area of low visibility enclosed within the 24 km isoline tends to follow the 50 N lat circle on both the 0000 and 1200 GMT analyses. However, the extent of the minimum region is greater in the 1200 GMT analysis, possibly indicating a diurnal effect. The 0900 GMT analysis, as with the July 0900 GMT analysis, shows a broad area of multiple local minima between 40° N lat and 65° N lat. Elsewhere on the analysis, gradients are chaotic and reflect the lower values of the intermediate time.

C. JANUARY

Figures 17b, 18a and 18b represent the 0000, 0900 and 1200 GMT density of transient ship observations in the study

area. As in comparable July analyses, the shipping lanes are evident on the 0000 and 1200 GMT analyses but are not discernible on the 0900 GMT analysis where only minor concentrations of observations appear near the coast of southern California and along the South Korean coast. The corresponding surface ship visibilities for 0000, 0900 and 1200 GMT are shown in Figs. 19a, 19b and 20a. The 0000 and 1200 GMT analyses are similar in character with isolines tending to follow latitude circles and gradients decreasing poleward. As was evident in prior months, the 0900 GMT analysis appears noisy with a much higher incidence of local maxima and minima. Figure 20b shows the standard deviations of the 0000 GMT surface visibilities. The highest values are in the Gulf of Alaska and are centered about a primary storm track. The region of lowest visibility values located near the Kamchatka Peninsula is also a region of low standard deviations. Interpretation is difficult here because of the sparse data of the region.

As Fig. 21a shows, the Aleutian low is the dominant feature in the North Pacific Ocean from coast to coast and from 35° N lat to the Arctic Ocean. In addition, anticyclones are present over Asia and in the eastern North Pacific Ocean between 20° N and 40° N lat. High pressure is also located in the central and western North Pacific Ocean between 20° N and 30° N lat. Generally, the central region of the Aleutian low is associated with the poorest visibility

because of precipitation and fog associated with the high number of migrating cyclones which pass through the region. Additionally, the powerful Asiatic anticyclone interacts with the Aleutian low in producing strong, cold northwesterly and westerly winds over much of the region. Cold air moving over relatively warmer ocean water is not a favorable situation for fog formation. Moving equatorward from the Aleutian low, both the 0000 and 1200 GMT visibility analyses show a gradient of increasing visibility, with maximum values in the regions located within the 20° N to 30° N lat belt of high pressure and associated stability.

Figures 21b and 22a show the 0000 and 1200 GMT frequency of visibility less than 2 km. The 0000 GMT analysis contains a minor maximum near Vladivostok, USSR, with the strongest and most extensive maximums on both analyses occurring in the southern coastal regions of the Kamchatka Peninsula and in the Bering Sea. The more significant maximums are generally colocated with the regions of the lowest mean visibilities previously discussed. The regions of high and low frequency are generally consistent for the 0000 and 1200 GMT analyses. Most differences are found in the magnitudes of the local maxima and minima. In the category less than 2 km, the 0000 GMT analysis contains a 30% maximum in the Bering Sea whereas the 1200 GMT contains a

10% maximum. This region is a primary storm track and tends to contain ice in winter. As a result, relatively few ships transit the area, making it a data-sparse region. Thus, differences in magnitudes of the maxima and minima may be due to differences in the number of observations received. The 2 to 10 km categories for 0000 and 1200 GMT are shown in Figs. 22b and 23a. The 0000 GMT analysis shows the highest frequency occurring in the region from the southeastern Kamchatka Peninsula through the Bering Sea into southwestern Alaska. The 10 percent isoline falls within the 35°-40° N lat circle which is roughly the southern boundary of the influence of the Aleutian low. Figures 23b and 24a show the remaining categories of visibility greater than or equal to 10 km for 0000 and 1200 GMT, respectively. Both analyses are consistent with the previous two frequency categories, showing the highest frequencies (best visibilities) south of 40° N lat with minimums in the Bering Sea and on the southern coasts of the Kamchatka Peninsula. Figure 24b shows the percent frequency of fog in any form. The low frequency of fog over the study area makes meaningful comparisons with the visibility analyses impossible. However, the low frequency of fog would indicate that fog alone may not be the dominant visibility restriction over the North Pacific Ocean in January or that the fog frequency analysis is in error in the areas of low visibility.

Figures 25a and 25b show 2400 LST and 0130 LST analyses for January. As in July, the inclusion of 0900 GMT data in the 2400 LST analysis is apparent by the chaotic gradients located east of 157.5° W long. The 0130 LST analysis, utilizing a three-hour blend of synoptic times, overcomes the effects of the 0900 GMT data. However, as with July, no attempt will be made to interpret the LST analyses.

D. APRIL

Figures 26a, 26b and 27a show 0000, 0900 and 1200 GMT surface visibility analyses. As with October, fairly high visibilities exist in all three analyses, with most values in the primary time analyses exceeding 16 km. Figure 27b shows the standard deviations for the 0000 GMT analysis. The zone of highest values is slightly south of the minimum visibility region. As in July, this displacement may indicate a greater variability of visibility values in the intermediate area between high and low visibility values. As in the other standard deviation analyses, sharp gradients poleward of 50° N lat and west of 170° W long may be related to the sparseness of data.

In comparing January and July climatology, it is apparent that April represents a transition month for the climate of the North Pacific Ocean. As Fig. 28a indicates, the Aleutian low has filled to nearly 1010 mb and extends from the

Kamchatka Peninsula into the Gulf of Alaska along 55° N. The intensifying Subtropical High is now 1022.5 mb and has a central region extending from near 30° N lat, 130° W long to 32° N lat, 178° E long. In this central region winds are light and variable. Elsewhere, southwesterly winds are becoming established throughout the region from 30° N to 55° N lat with the exception being the North American coast where northerly winds exist. Easterly winds are found equatorward of 30° N lat throughout the region. The highest visibilities exist in the eastern periphery of the Subtropical High and equatorward of 30° N where north and northeast winds in combination with underlying warm water create stable atmospheric conditions. Poleward of 30° N lat visibility gradually decreases and minimum regions extend as far south as 45° N lat. The 0900 GMT analysis is consistent with the previously described intermediate analyses in that gradients are chaotic with a distinct difference in character from the 0000 and 1200 GMT analyses. The minimum regions in both primary-time analyses are located within or adjacent to the primary storm tracks for April, particularly the regions west of the Kamchatka Peninsula and in the south-central Bering Sea. A slight diurnal effect may be evident in that the low visibility regions in the 1200 GMT analysis are more extensive than for the 0000 GMT analysis. This is apparent for the region contained within each isoline,

especially the 20 km isoline. As with July and October, a significant climatic factor is the presence of southwesterly winds over the western North Pacific Ocean. April represents a transition month of westerly to southwesterly winds over the region west of 150° W and poleward of 30° N. The poleward transport of warmer air over colder water, leads to increased fog formation. Figure 28b shows the frequency of occurrence of fog for April. The figure shows a considerable increase in extent over the January frequency. The areas of increased frequency, primarily poleward of 40° N lat, are consistent with the regions of poorest visibility on the surface visibility analyses. This consistency may indicate the increasing influence of fog upon visibility restrictions with a minimal influence existing in October and January, an intermediate influence present in April and a maximum influence existing in July.

V. CONCLUSIONS AND SUGGESTIONS FOR FURTHER STUDY

A surface visibility climatology is an important tool for both military and civilian operational users and planners. This study, with the application of an objective analysis routine, has transformed a 20-year data set for the North Pacific Ocean into a meaningful climatology. Using a seasonal approach, the analyses produced show that July (summer) is the period of significant visibility restrictions and January (winter) has comparatively fewer restrictions. The autumn and spring periods, represented by October and April, show intermediate visibility restrictions. Comparisons between the visibility analyses and a fog frequency climatology indicate that fog has a minimal influence upon visibility restrictions in October and January, an intermediate influence in April and a maximal influence in July.

Some support for diurnal variations in visibility was revealed by the regional comparisons made between the primary-synoptic time mean surface visibilities and the fog frequency occurrence analyses for July. Other support consists of numerous analyses which show poorer visibility for 1200 GMT than for comparable 0000 GMT analyses. While this support exists for diurnal variations in visibility over

the North Pacific Ocean, the discovery of and investigation into the intermediate synoptic time low-visibility bias precludes a more detailed investigation into diurnal visibility changes.

The following recommendations are offered for future study:

1. To further enrich the data base, combine available Ocean-Weather-Station observations with those from transient ships.
2. Initialize all near-ocean land stations with climatological values for the field being analyzed. Such an initialization may lessen the discontinuity often apparent between the initial first-guess values used over land with the actual values present over ocean.
3. As an alternative to (2) above, initialize the major ocean-land boundaries with values extracted from climatological summaries of coastal regions. Hopefully, this initialization would allow a more accurate coastal visibility depiction.
4. Compare satellite-observed low clouds to the primary-time visibility climatologies to aid in determining the exact nature of diurnal variations in visibility.
5. The investigation into the intermediate-time bias should be extended to include the examination of a number of transient ship weather logs or the weather reporting

history of these ships. This examination may reveal differences between primary and secondary time observations.

TABLE I

Transient ship observations for January, April, July and October. These represent 20 years of observations (1954-1973) over the North Pacific Ocean study area (20° N - 70° N lat, 120° E - 110° W long).

GMT	January	April	July	October	Totals
0000	81668	85781	90302	93965	351716
0300	14615	16139	19323	18442	68519
0600	76993	82990	86018	84810	330811
0900	11686	13073	16255	14499	55513
1200	73648	78649	81318	80784	314399
1500	14003	14782	17027	19942	65754
1800	76754	82703	84731	84632	328820
2100	16769	17683	20445	19942	74839
Totals	366136	391800	415419	417016	1590371

TABLE II

July band averaged (weighted mean) surface visibilities for the North Pacific Ocean area 20° N - 70° N lat.

	(a) Entire region		(b) 120° E - 180° long		(c) 180° - 110° W long	
GMT	Mean Visibility (km)	Total Observations	Mean Visibility (km)	Total Observations	Mean Visibility (km)	Total Observations
0000	29.5	90302	27.7	33921	30.5	56381
0300	24.5	19323	23.5	10471	25.8	8852
0600	28.8	86018	28.4	33065	29.0	52953
0900	22.7	16255	22.1	9810	23.4	6445
1200	27.6	81318	26.4	31453	28.3	49865
1500	21.0	17027	20.3	8229	21.8	8798
1800	28.1	84731	26.3	30345	29.1	54386
2100	23.5	20445	21.8	9198	24.9	11247

TABLE III

July band averaged surface visibilities (weighted means) 40° N - 50° N lat, 120° E - 180° long, for 3-hourly local standard times (LST) with contributing GMT-time mean visibilities and corresponding observation totals.

				GMT Contributor			GMT Contributor	
LST	Mean Visibility (km)	Number of Observations	GMT	Mean Visibility (km)	Number of Observations	GMT	Mean Visibility (km)	Number of Observations
0000	11.8	5420	1500	11.5	723	1200	11.8	4697
0300	12.0	3498	1800	15.1	1894	1500	8.3	1604
0600	11.6	5494	2100	13.2	841	1800	11.3	4653
0900	14.4	4076	0000	17.5	2356	2100	10.0	1720
1200	14.1	6046	0300	15.6	1067	0000	13.8	4979
1500	15.3	4116	0600	17.9	2380	0300	11.6	1736
1800	13.8	5922	0900	14.2	994	0600	13.7	4928
2100	12.9	3855	1200	16.6	2099	0900	9.6	1756

TABLE IV

July band averaged surface visibilities (weighted means) 40° N - 50° N lat, 180° to 110° W long, for 3-hourly local standard times (LST) with contributing GMT-time mean visibilities and corresponding observation totals.

			GMT Contributor			GMT Contributor		
LST	Mean Visibility (km)	Number of Observations	GMT	Mean Visibility (km)	Number of Observations	GMT	Mean Visibility (km)	Number of Observations
0000	17.0	5017	1200	15.8	4089	0900	22.1	928
0300	23.8	7371	1500	15.5	392	1200	24.3	6969
0600	17.6	5647	1800	15.9	4091	1500	22.3	1556
0900	25.2	7955	2100	16.9	437	1800	25.6	7518
1200	20.1	5969	0000	18.5	4334	2100	24.4	1635
1500	27.1	8463	0300	17.8	439	0000	27.6	8024
1800	18.9	5795	0600	16.9	4372	0300	25.6	1423
2100	24.5	7716	0900	16.9	390	0600	24.9	7326

TABLE V

July band averaged surface visibilities for
20° N lat to 30° N lat, 120° E long to 180° long
and
50° N lat to 60° N lat, 120° E long to 180° long.

GMT	20° N lat to 30° N lat 120° E long to 180° long		50° N lat to 60° N lat 120° E long to 180° long	
	Mean Visibility (km)	Total Observations	Mean Visibility (km)	Total Observations
0000	35.7	11760	16.6	2470
0300	33.4	3459	15.2	1157
0600	36.4	11410	17.5	2240
0900	33.1	3133	13.8	1226
1200	34.1	10988	14.5	2025
1500	30.3	2722	12.3	994
1800	34.3	10614	14.2	1937
2100	32.0	3078	11.9	1147

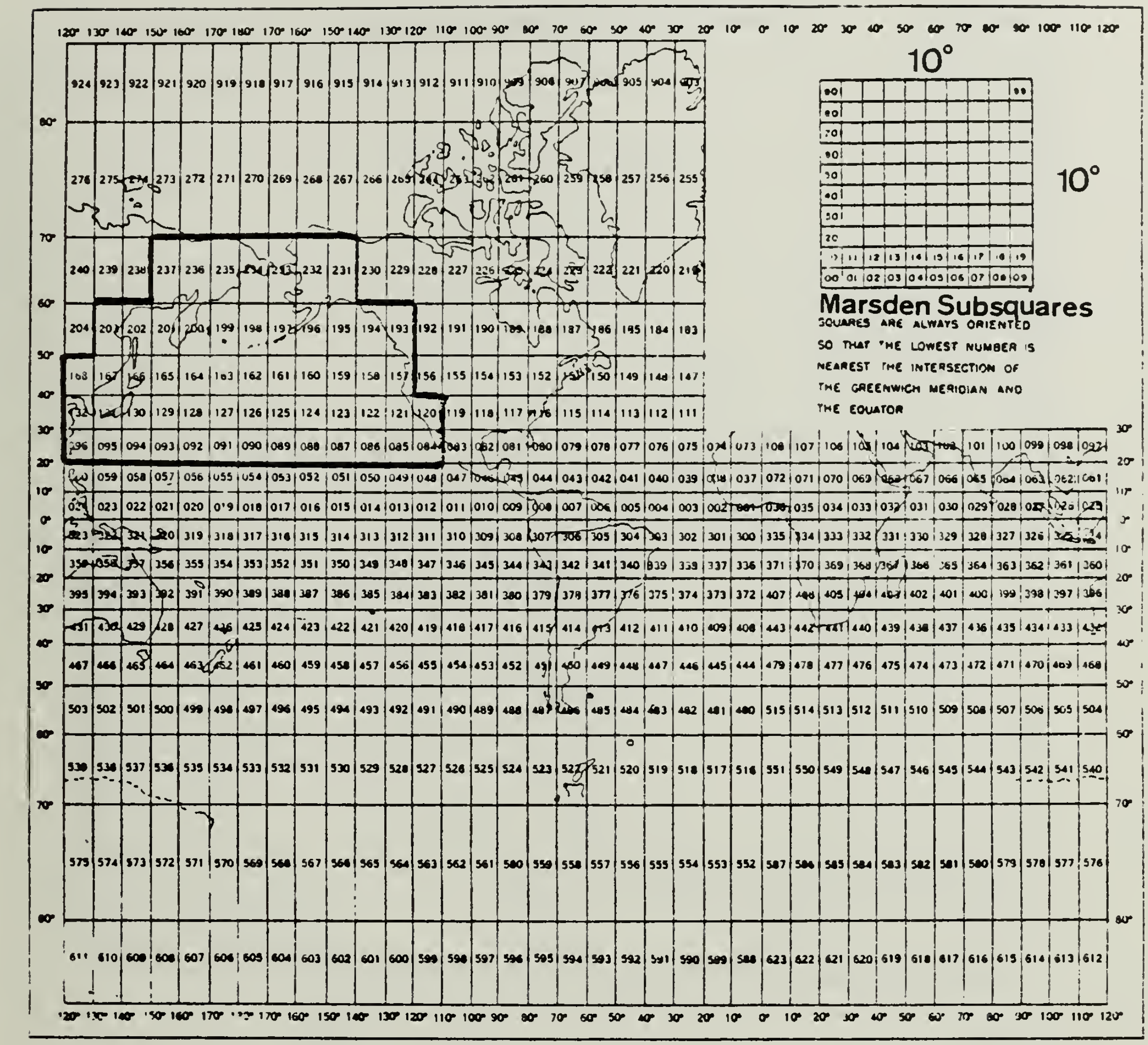

Figure 1. Global Network of Marsden squares with outline of squares comprising the study area.

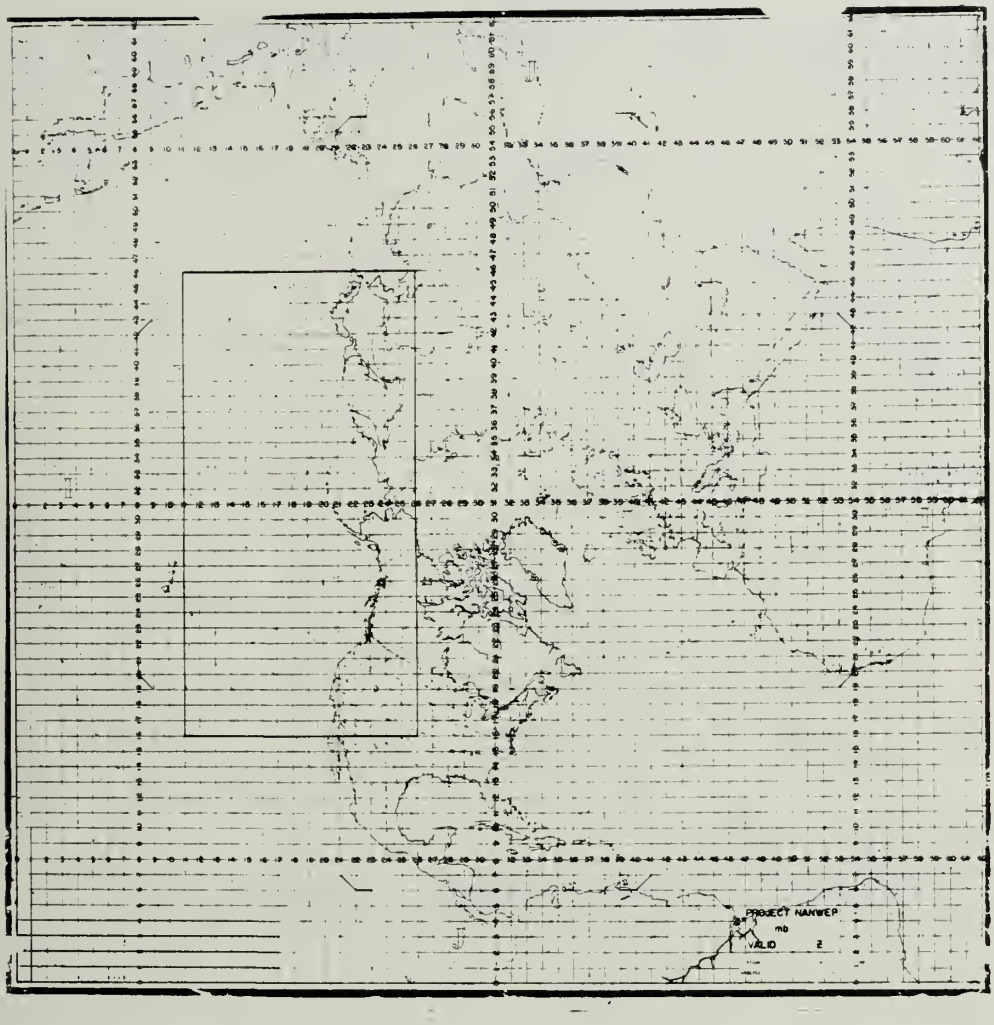

Figure 2. FNOC's 63x63 grid, with outline of North Pacific Ocean rectangular grid area used in study.

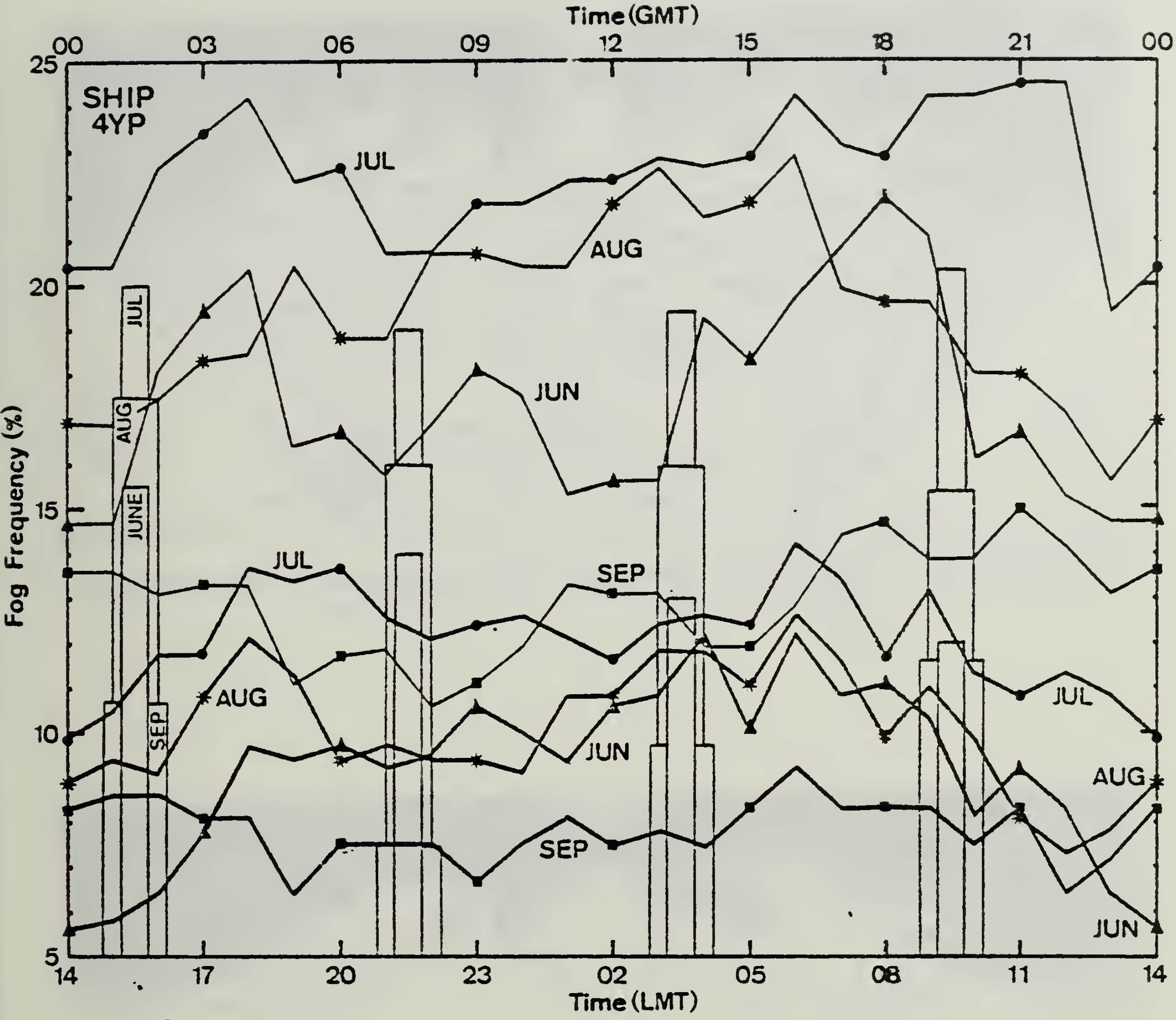

Figure 3. Diurnal fog frequencies for North Pacific Ocean Weather-Station Papa (50° N, 145° W). Dense fog, visibility less than 1 km (heavy solid lines). Dense and light fog, visibility less than 10 km (light solid lines) (Renard, 1976). Histograms represent percent frequency of fog (without precipitation), (U.S. Naval Weather Service Environmental Detachment, 1974).

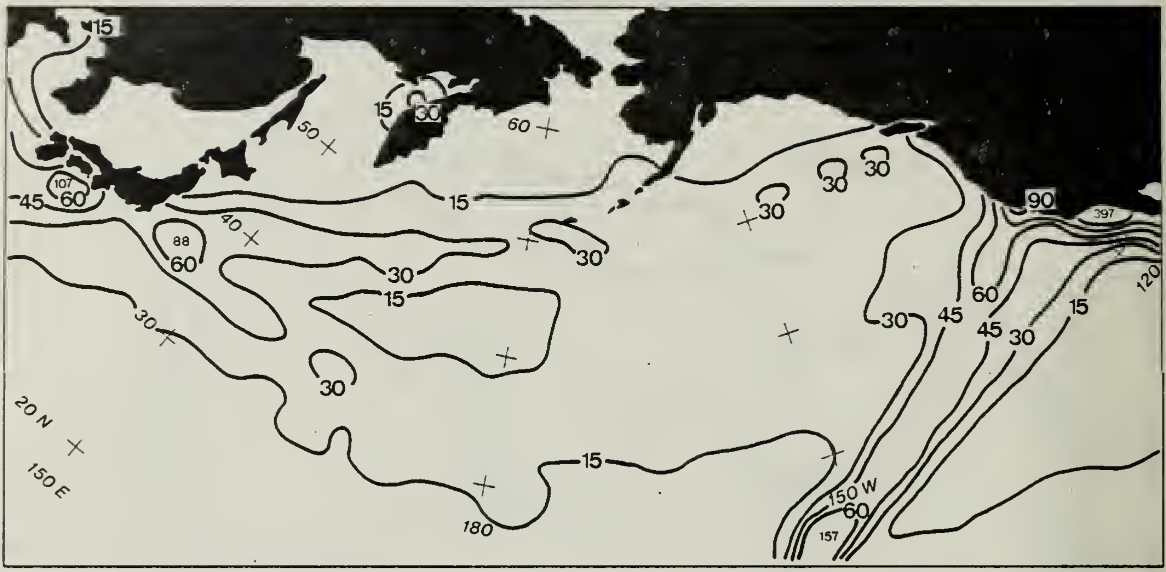

Figure 4a. July 0000 GMT Marsden subsquare transient ship density.

Figure 4b. Same as 4a for 0900 GMT.

Figure 5a. July 1200 GMT Marsden subsquare transient ship density.

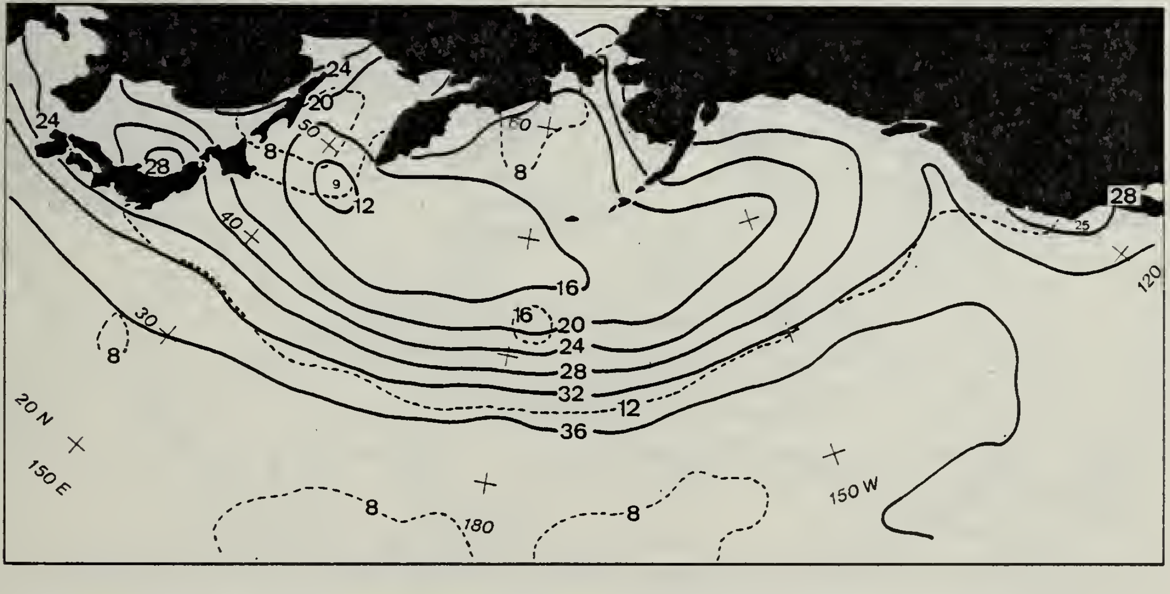

Figure 5b. July 0000 GMT mean surface visibility (km) (solid lines) and standard deviations at 4 km intervals (dashed lines).

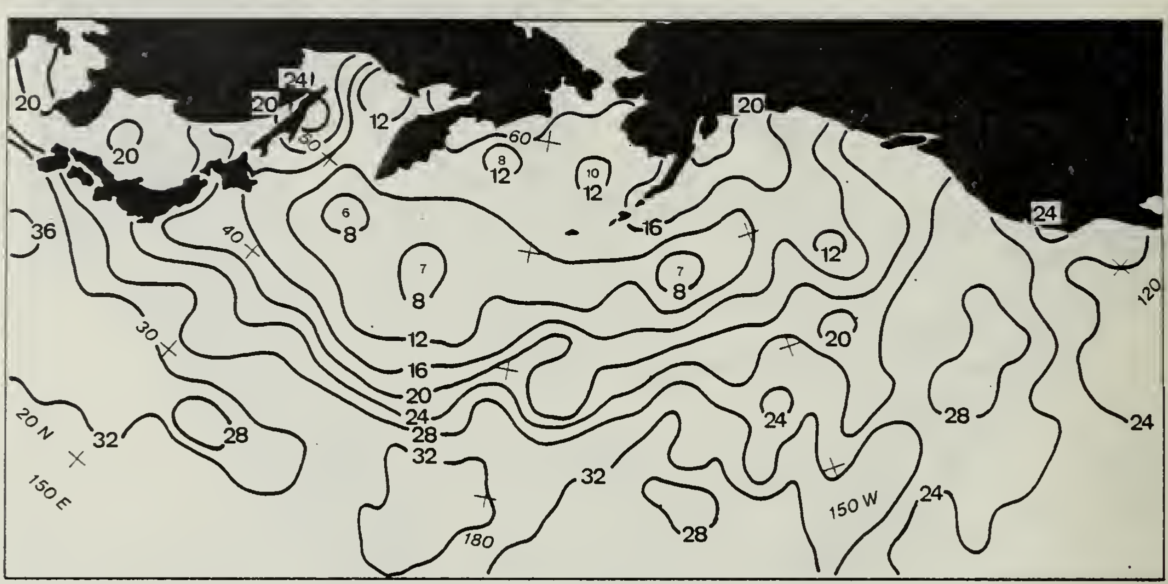

Figure 6a. July 0900 GMT mean surface visibility (km).

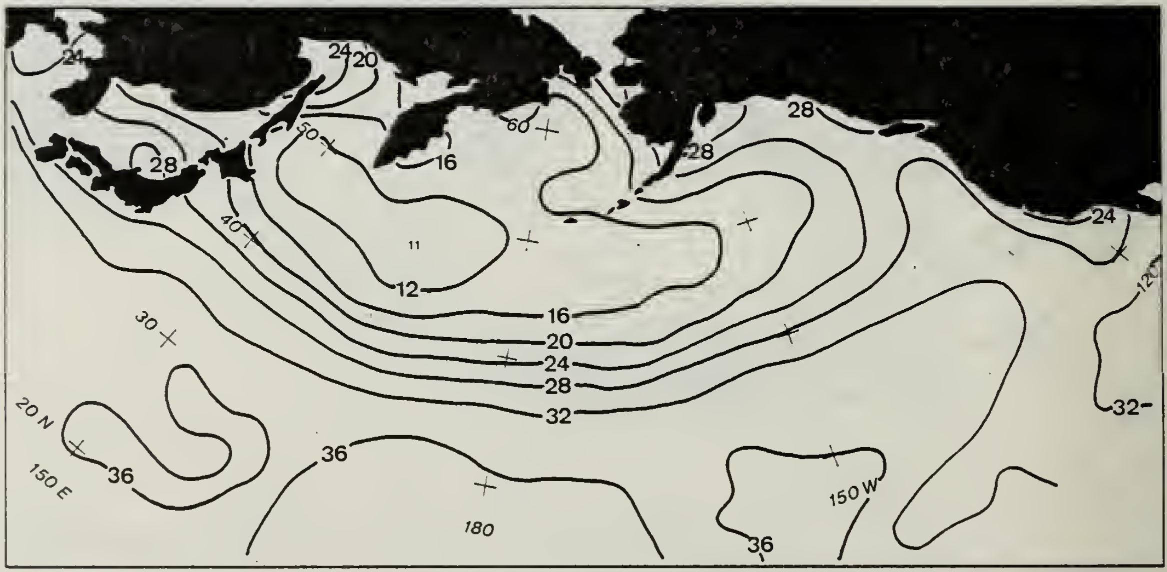

Figure 6b. Same as 6a for 1200 GMT (km).

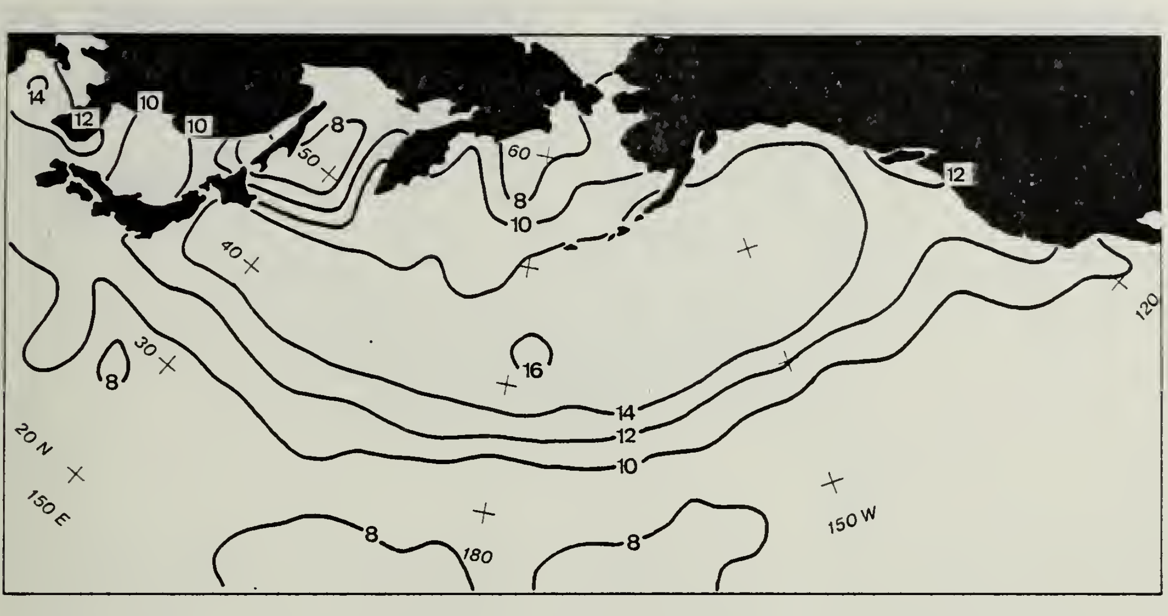

Figure 7a. July 0000 GMT standard deviations of surface visibility (km).

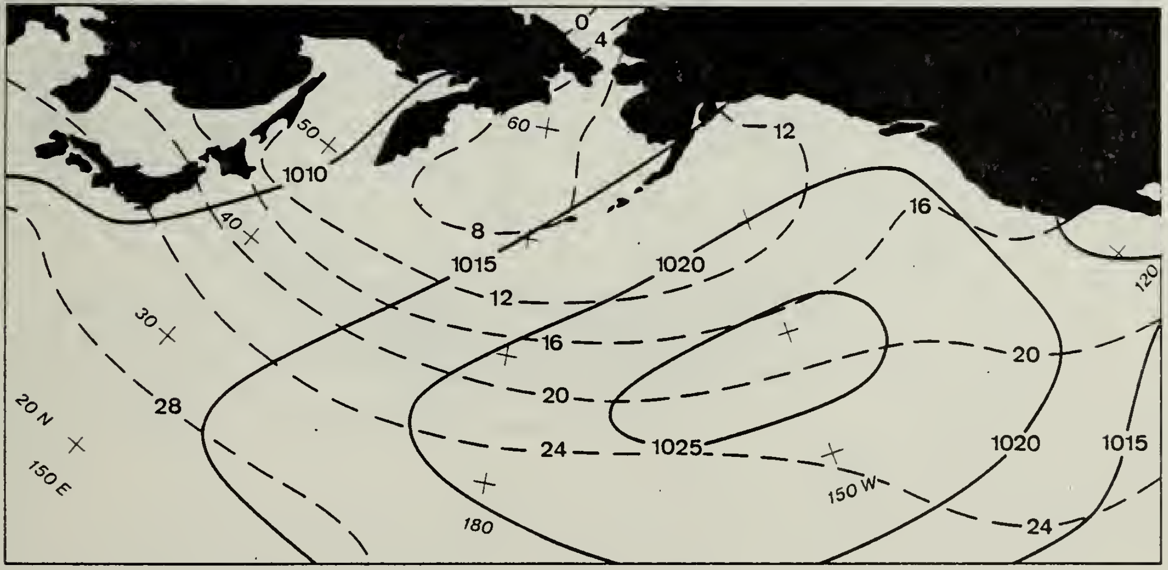

Figure 7b. July mean sea-level pressure (mb) (solid lines) and mean sea-surface temperatures (°C) (dashed lines) for the North Pacific Ocean, (U.S. Naval Weather Service Environmental Detachment, 1977).

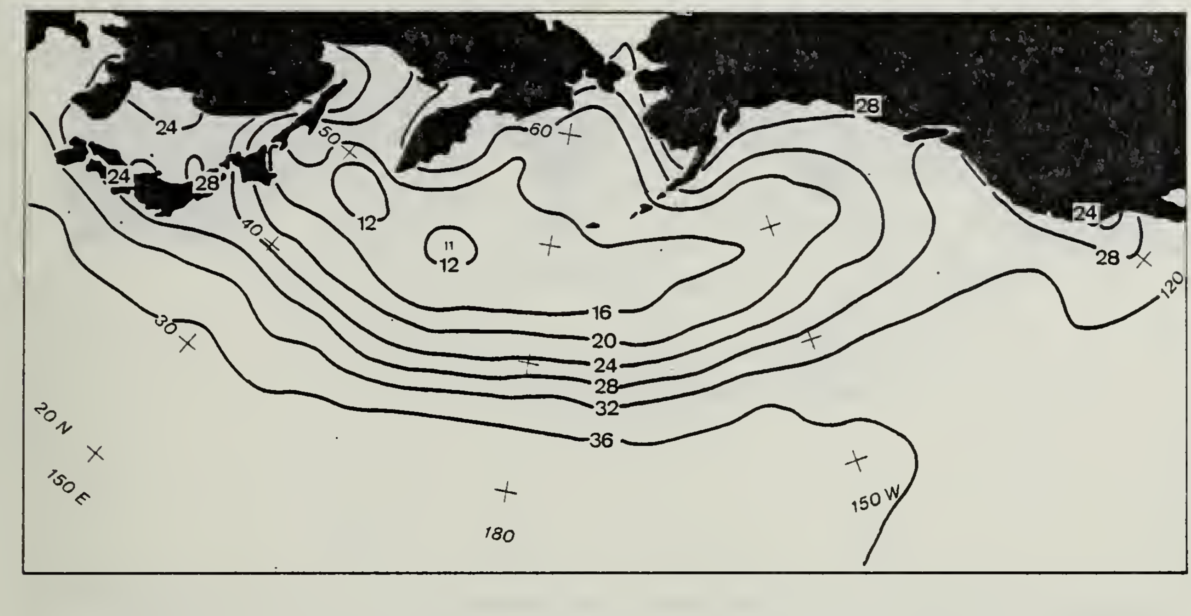

Figure 8a. July 0600 GMT mean surface visibility (km).

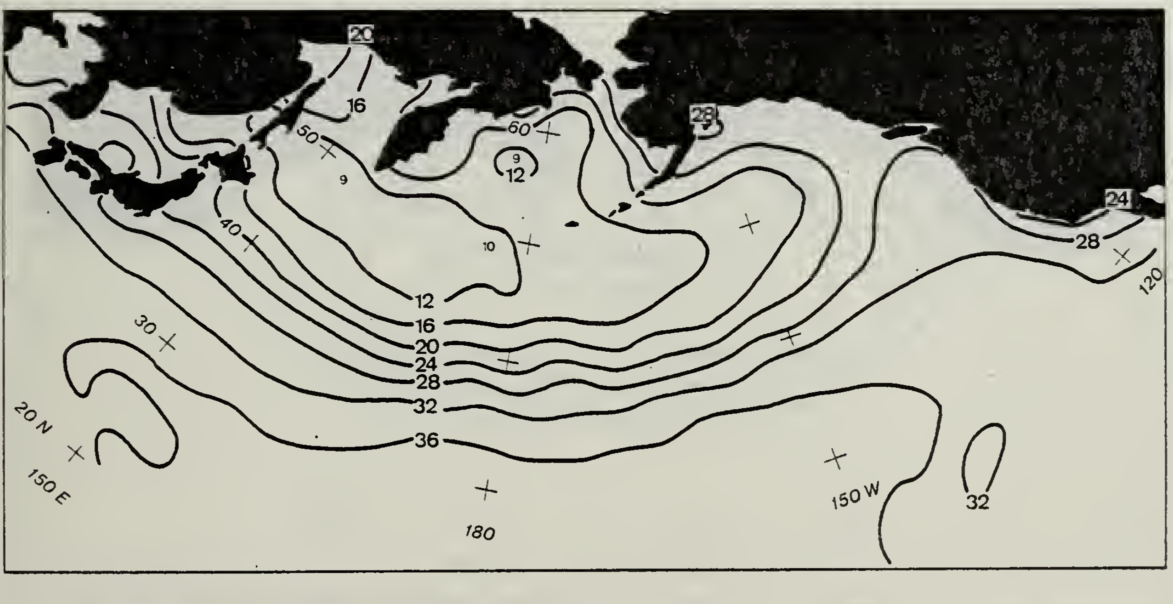

Figure 8b. Same as 8a for 1800 GMT.

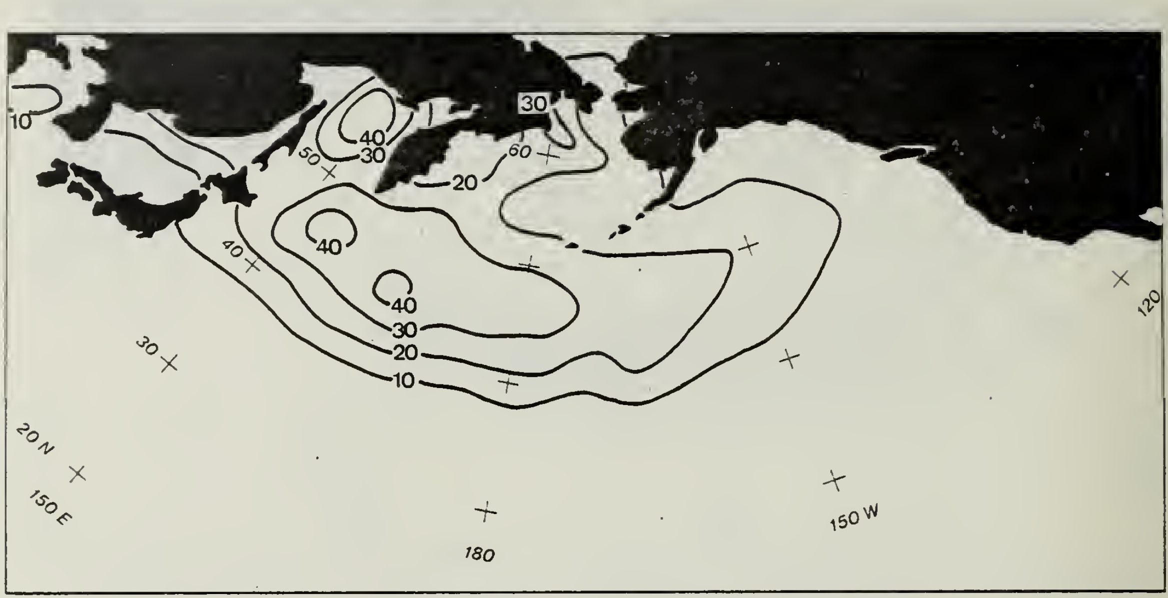

Figure 9a. July 0000 GMT frequency of visibility less than 2 km (%).

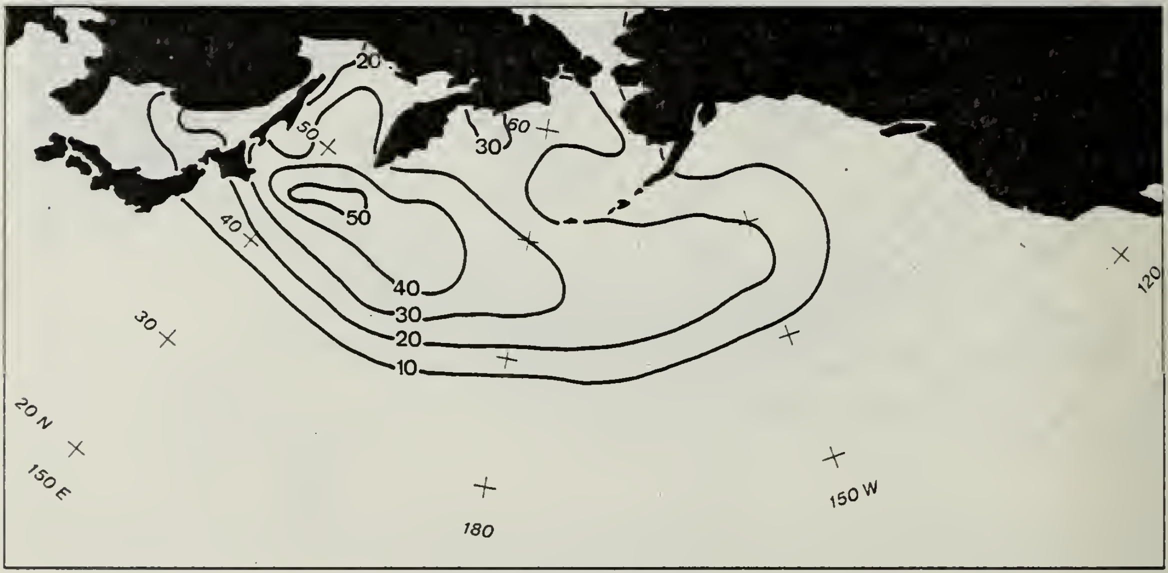

Figure 9b. Same as 9a for 1200 GMT.

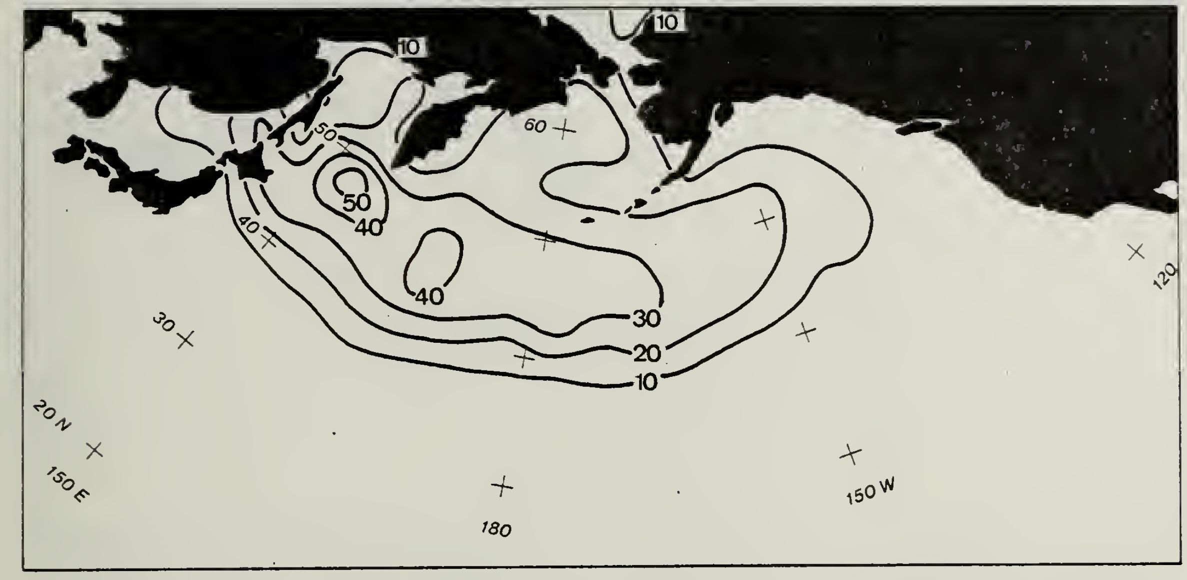

Figure 10a. July 0600 GMT frequency of visibility less than 2 km (%).

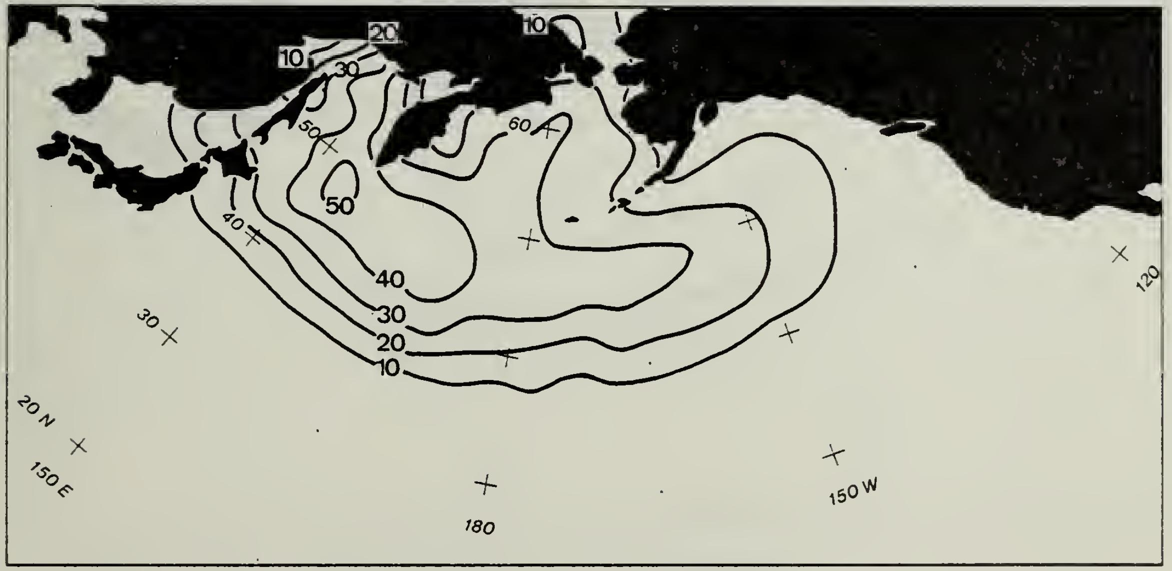

Figure 10b. Same as 10a for 1800 GMT.

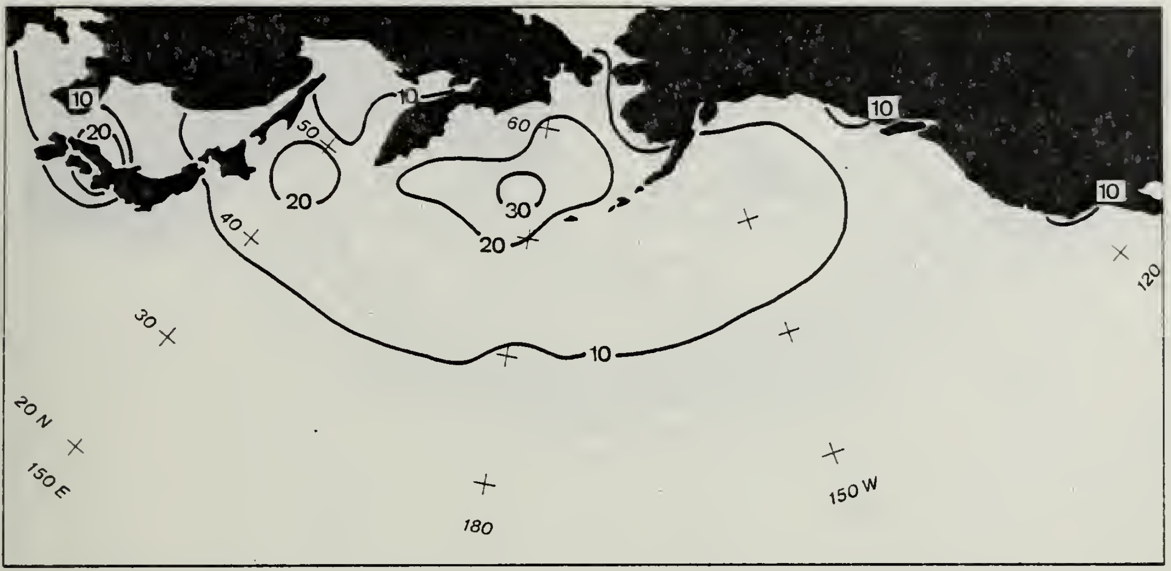

Figure 11a. July 0000 GMT frequency of visibility equal to or greater than 2 km and less than 10 km (%).

Figure 11b. Same as 11a for 1200 GMT.

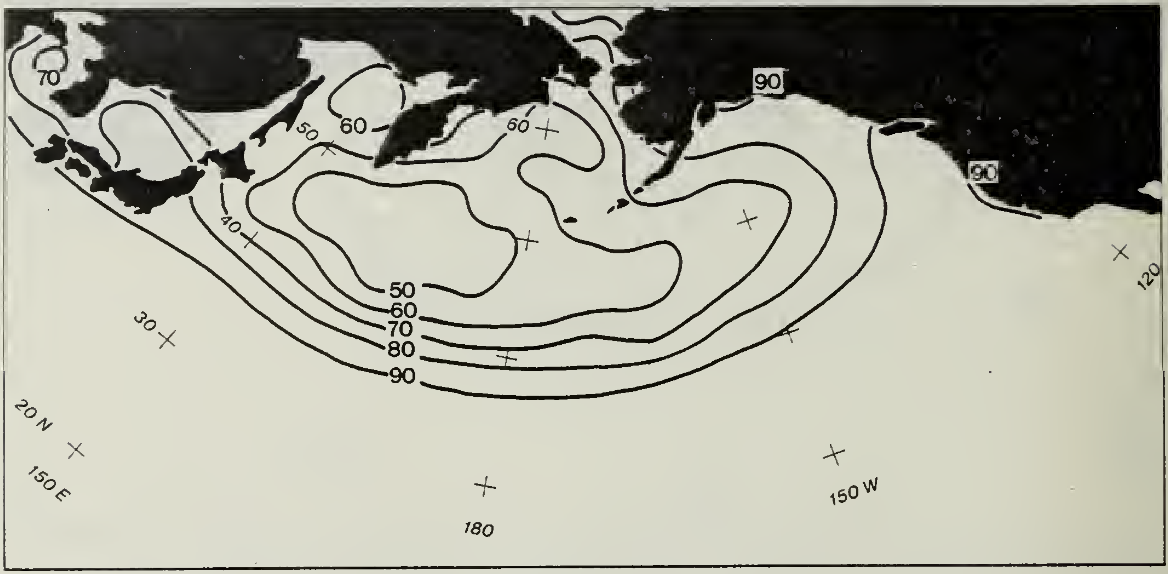

Figure 12a. July 0000 GMT frequency of visibility equal to or greater than 10 km (%).

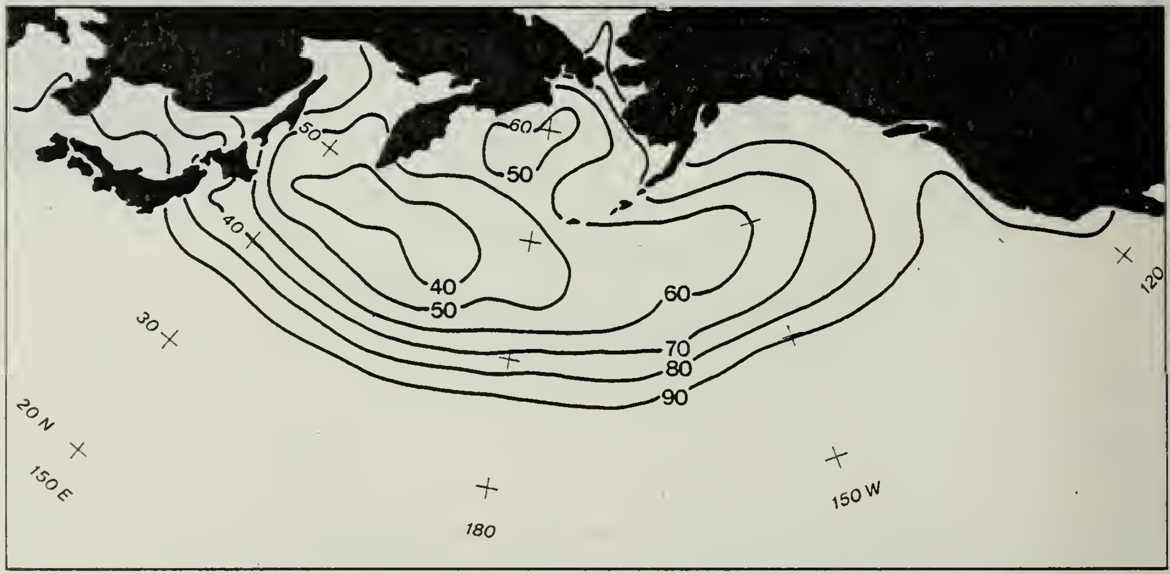

Figure 12b. Same as 12a for 1200 GMT.

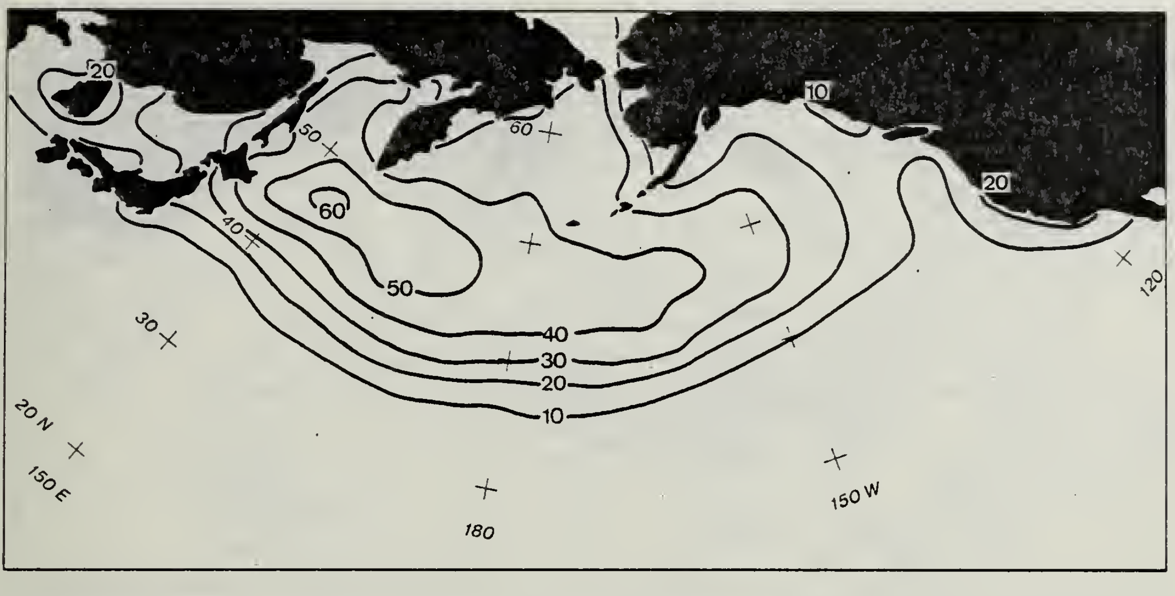

Figure 13a. July frequency of fog occurrence (%).

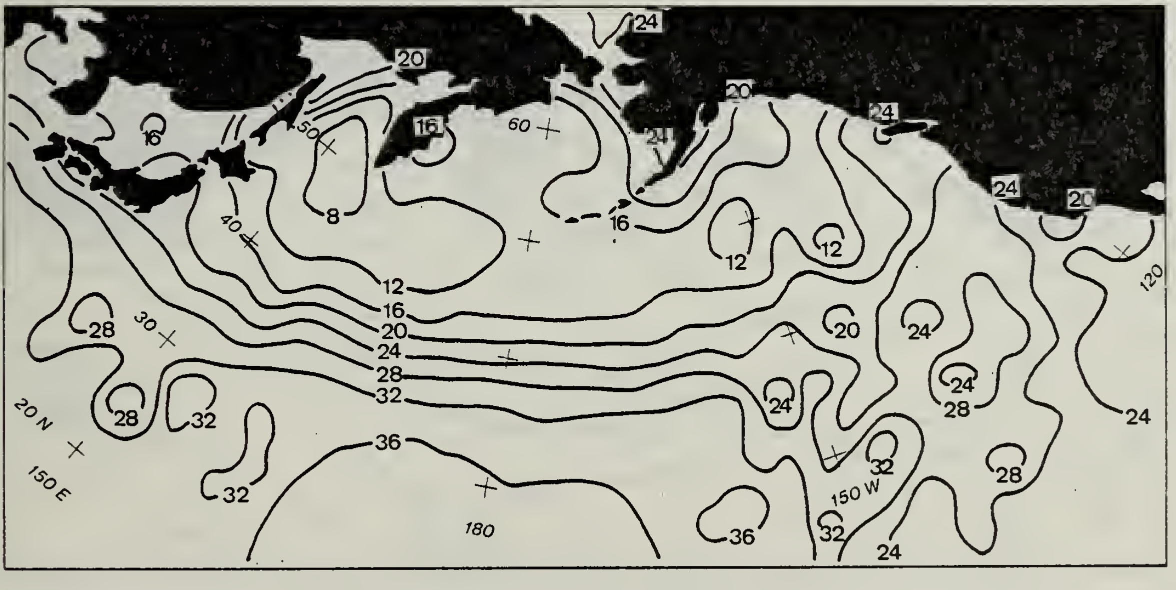

Figure 13b. July 0000 local standard time (LST) mean surface visibility (km).

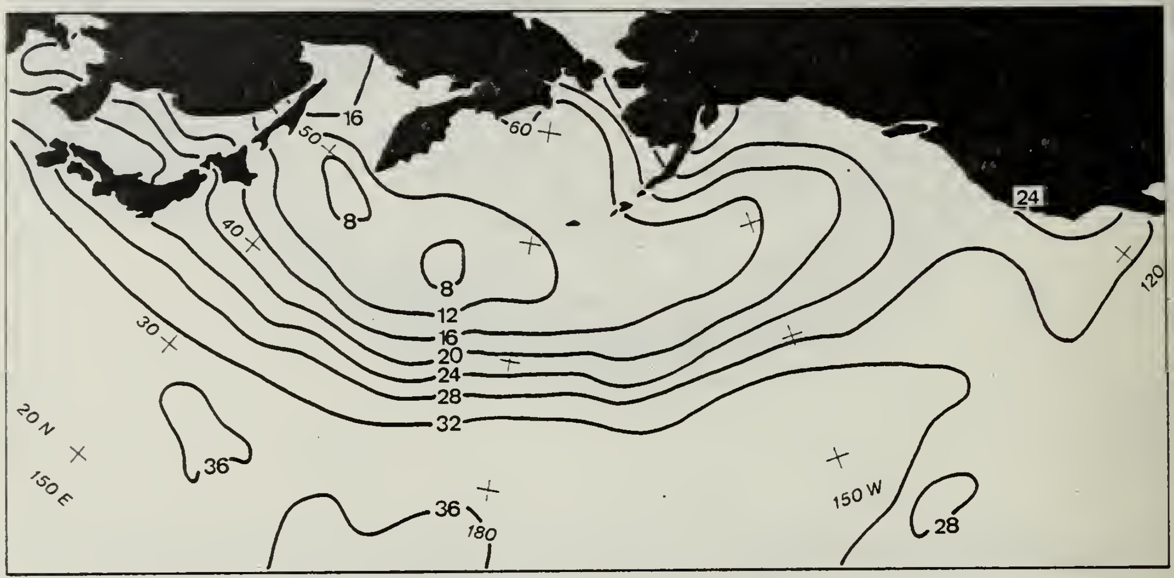

Figure 14a. July 0130 LST mean surface visibility (km).

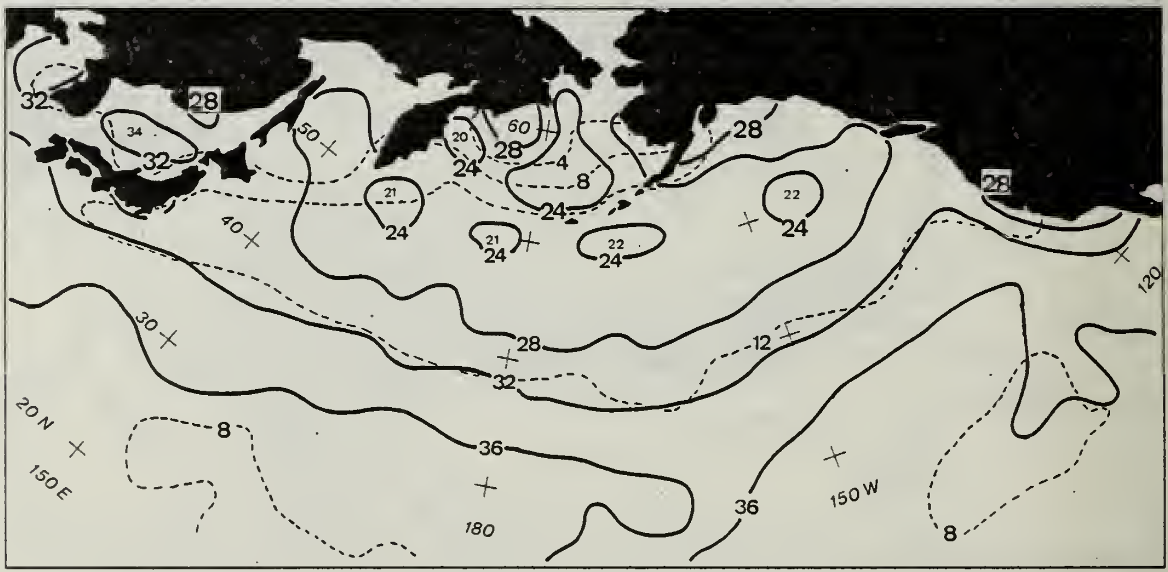

Figure 14b. October 0000 GMT mean surface visibility (km) (solid lines) and standard deviations at 4 km intervals (dashed lines).

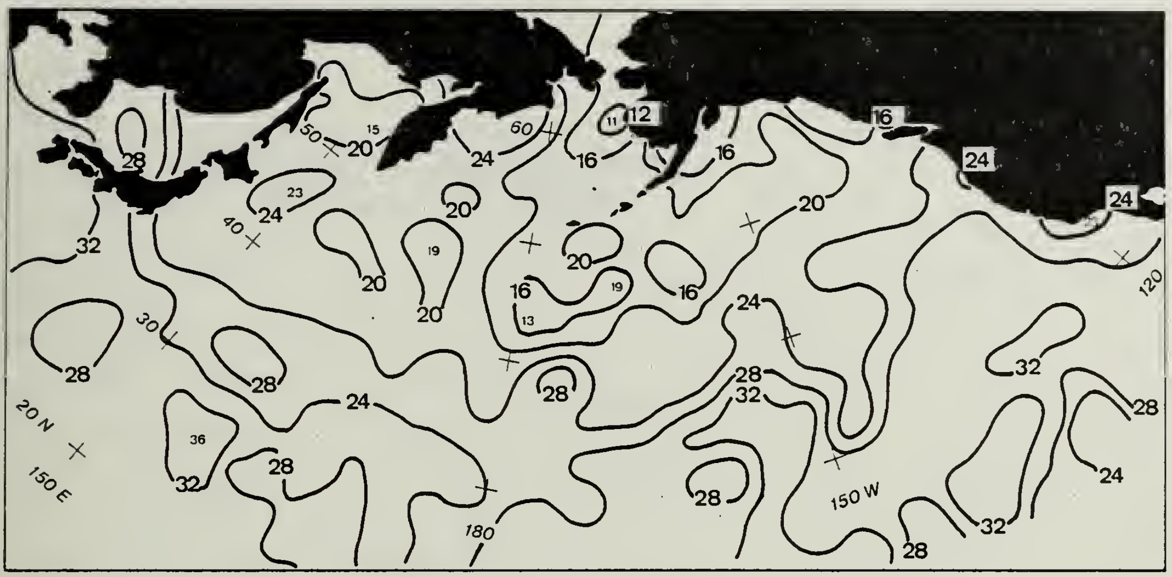

Figure 15a. October 0900 GMT mean surface visibility (km).

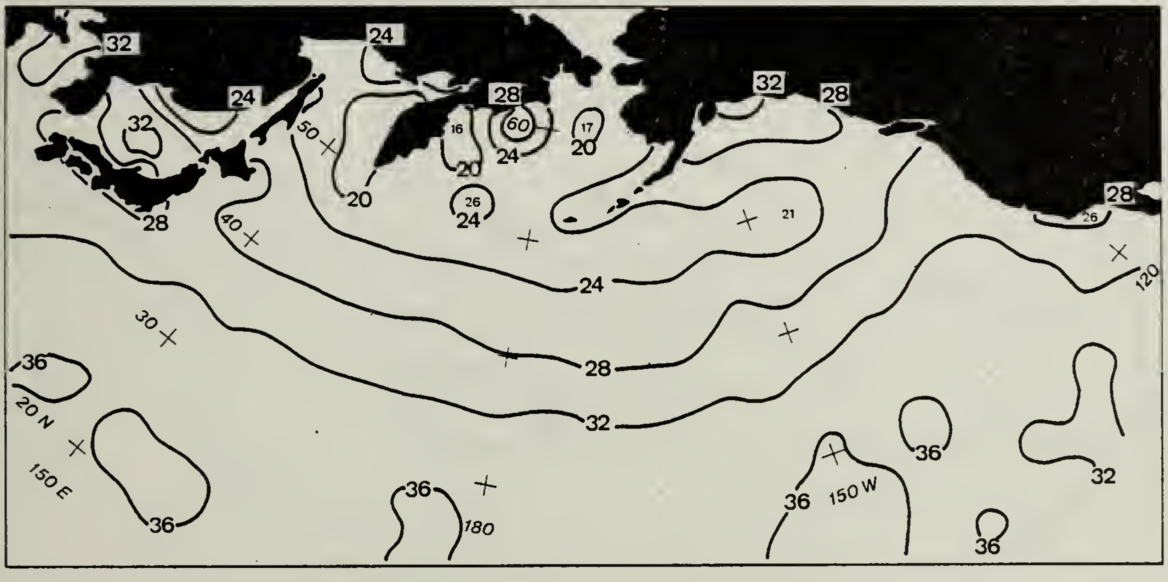

Figure 15b. Same as 15a for 1200 GMT.

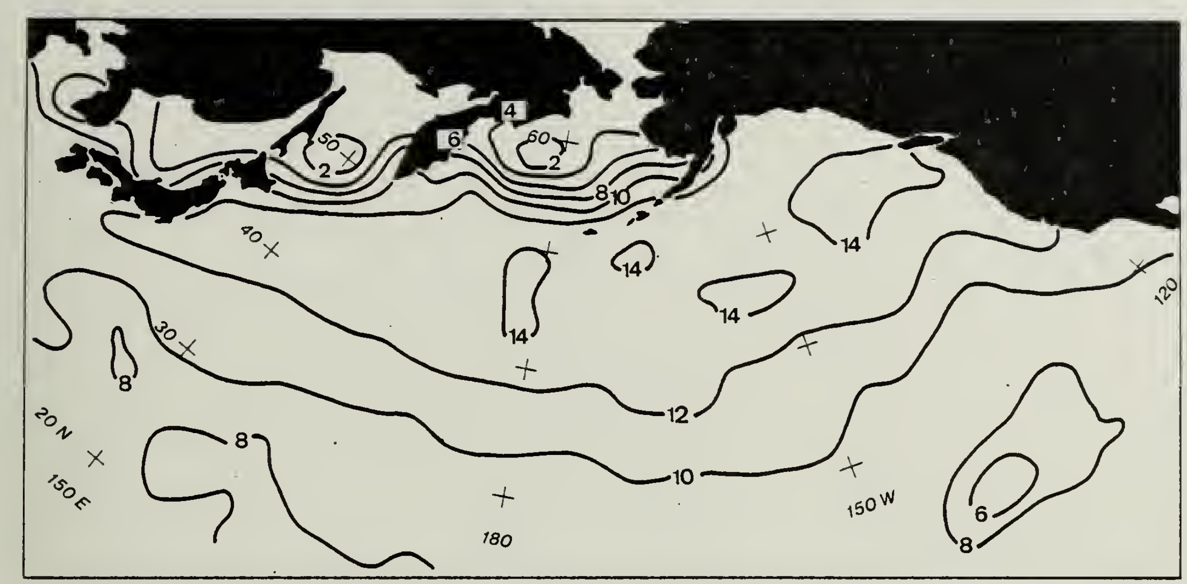

Figure 16a. October 0000 GMT standard deviations of mean surface visibility (km).

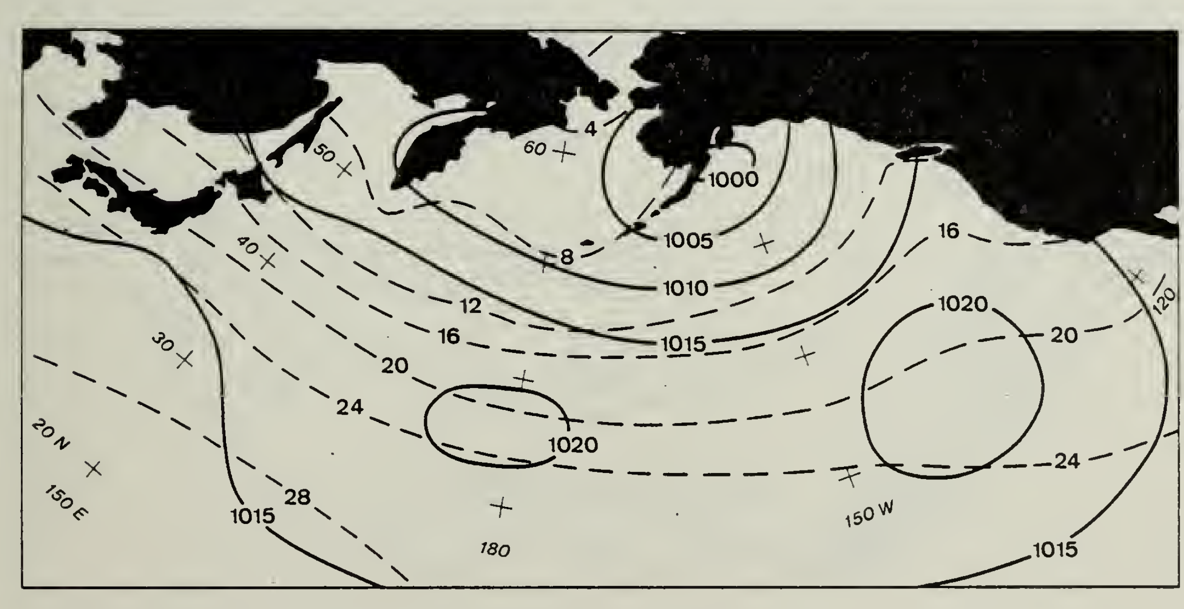

Figure 16b. October mean sea-level pressures (mb) (solid lines) and sea-surface temperatures (°C) (dashed lines) for the North Pacific Ocean, (U.S. Naval Weather Service Environmental Detachment, 1977).

Figure 17a. October frequency of fog occurrence (%).

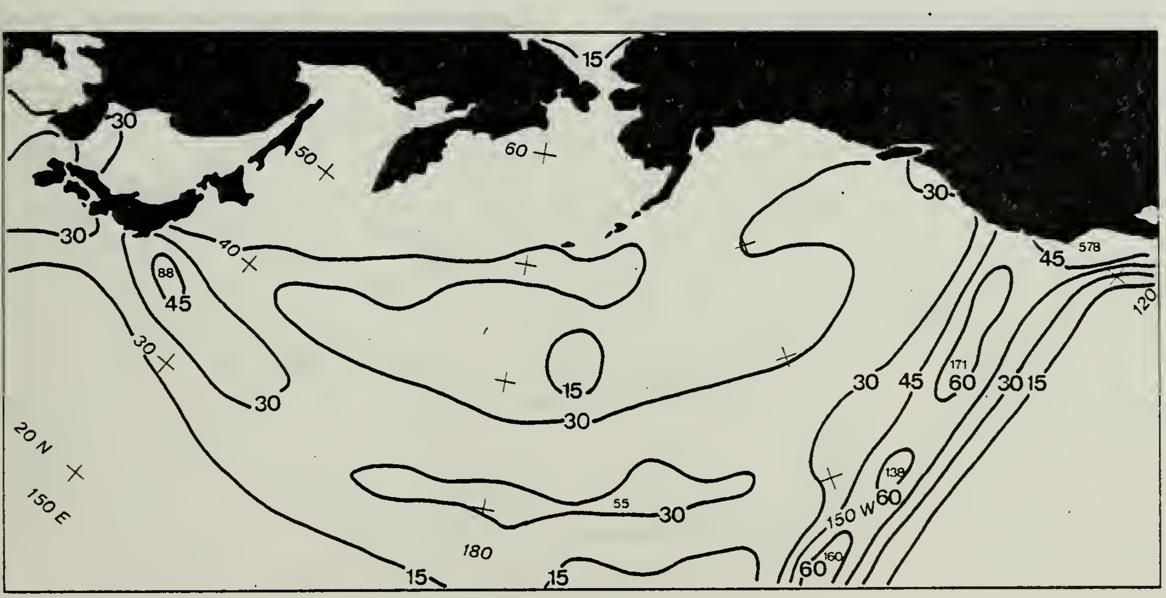

Figure 17b. January 0000 GMT Marsden subsquare transient ship density.

Figure 18a. January 0900 GMT Marsden subsquare transient ship density.

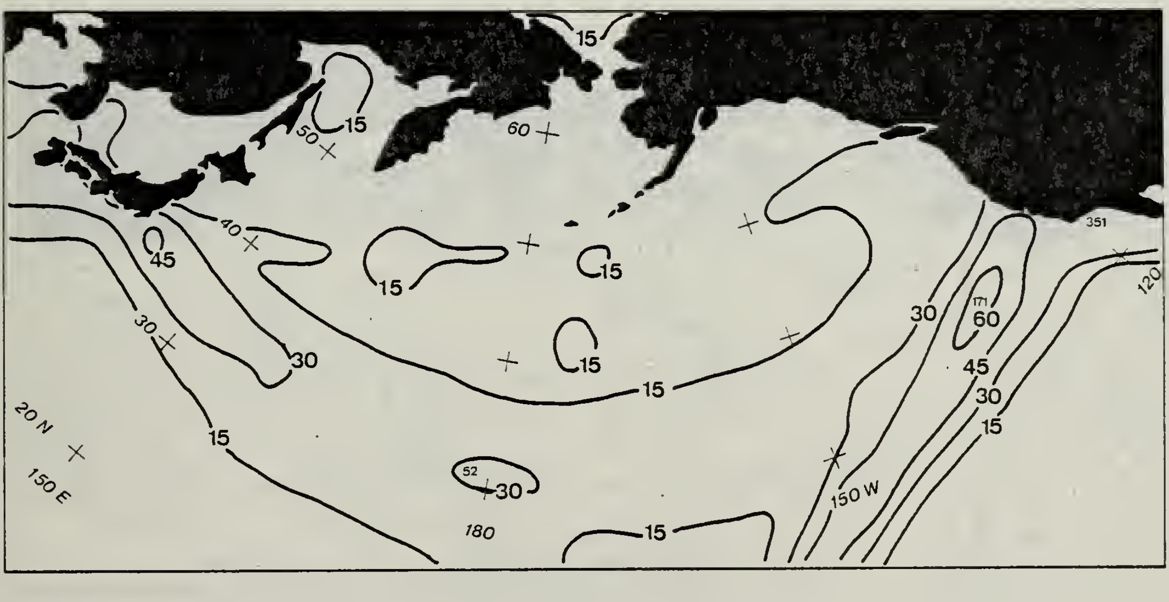

Figure 18b. Same as 18a for 1200 GMT.

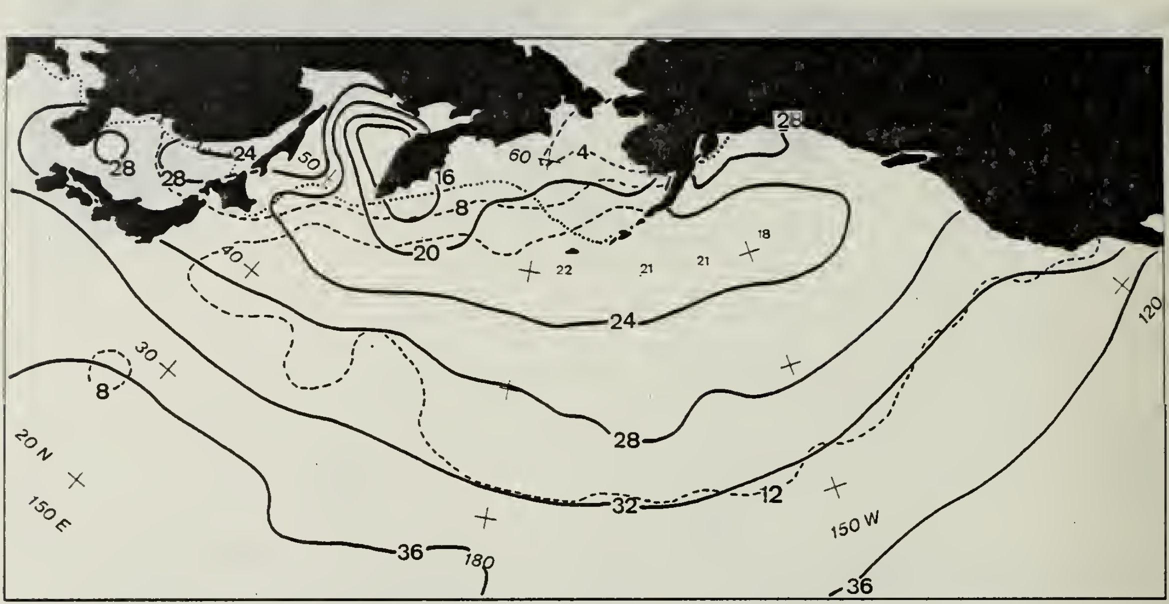

Figure 19a. January 0000 GMT mean surface visibility (km) (solid lines), standard deviations at 4 km (dashed lines), maximum southern extent of ice coverage .1 or greater (dotted line), (U.S. Naval Weather Service Environmental Detachment, 1977).

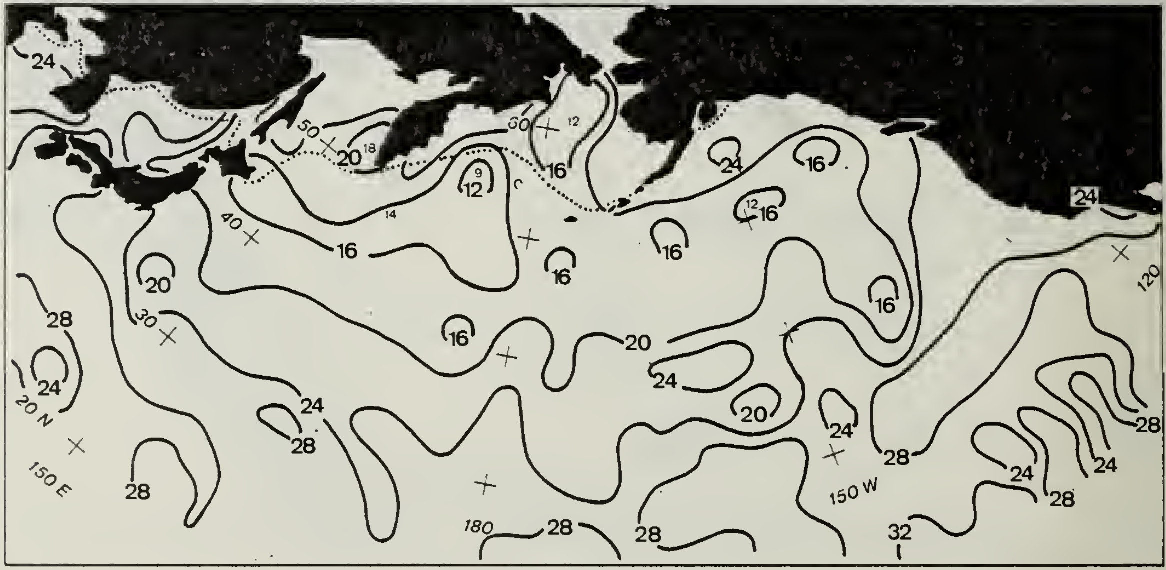

Figure 19b. January 0900 GMT mean surface visibility (km) (solid lines), maximum southern extent of ice coverage .1 or greater (dotted line), (U.S. Naval Weather Service Environmental Detachment, 1977).

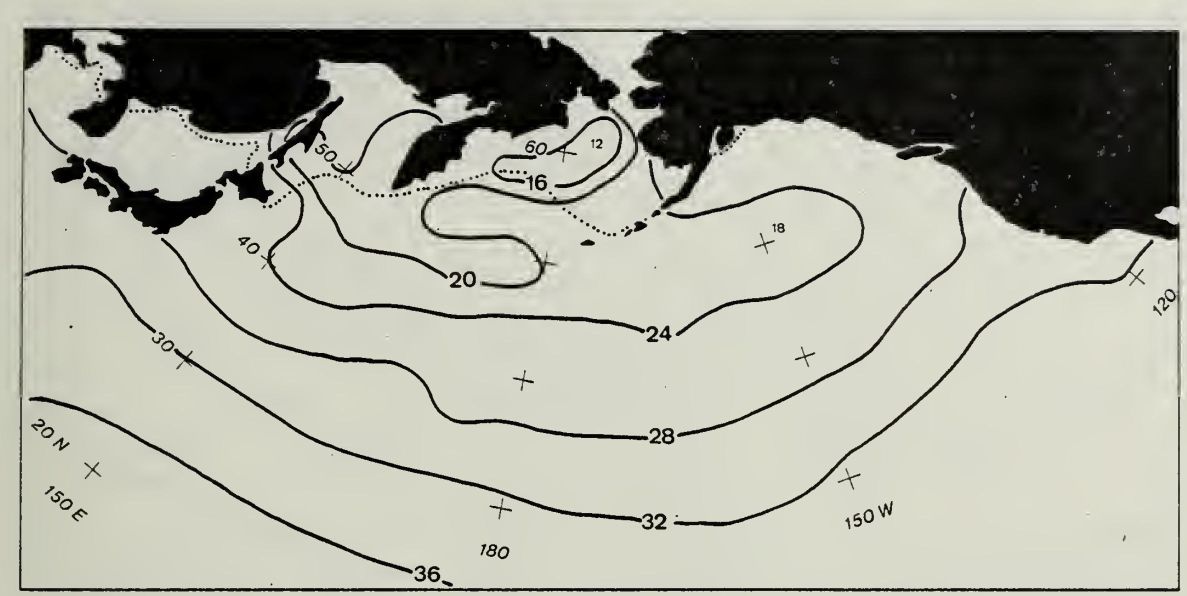

Figure 20a. January 1200 GMT mean surface visibility (km) (solid lines), maximum southern extent of ice coverage .1 or greater (dotted line), (U.S. Naval Weather Service Environmental Detachment, 1977).

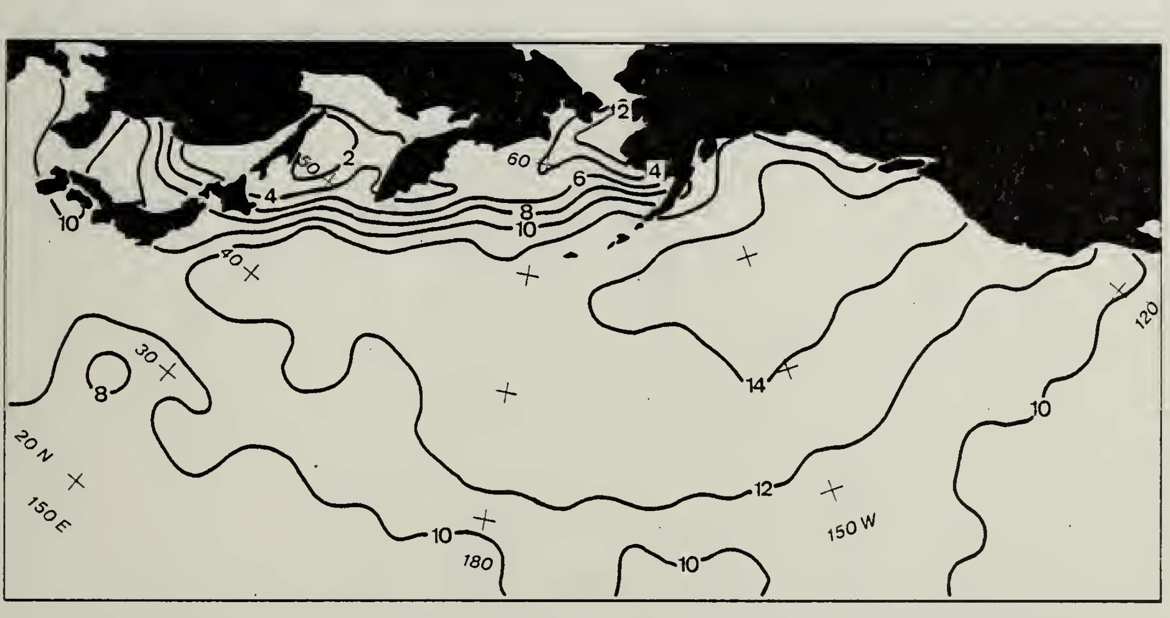

Figure 20b. January 0000 GMT standard deviations of surface visibility (km).

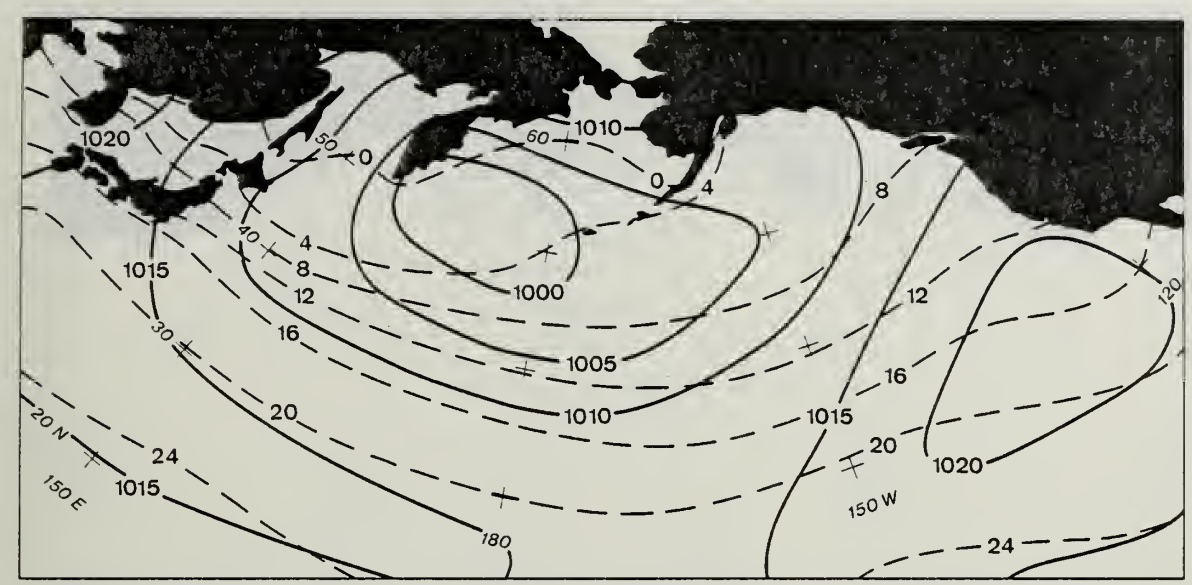

Figure 21a. January mean sea-level pressures (mb) (solid lines), sea-surface temperatures (°C) (dashed lines) for the North Pacific Ocean, (U.S. Naval Weather Service Environmental Detachment, 1977).

Figure 21b. January 0000 GMT frequency of visibility less than 2 km (solid lines) (%), maximum southern extent of ice coverage .1 or greater (dotted line), (U.S. Naval Weather Service Environmental Detachment, 1977).

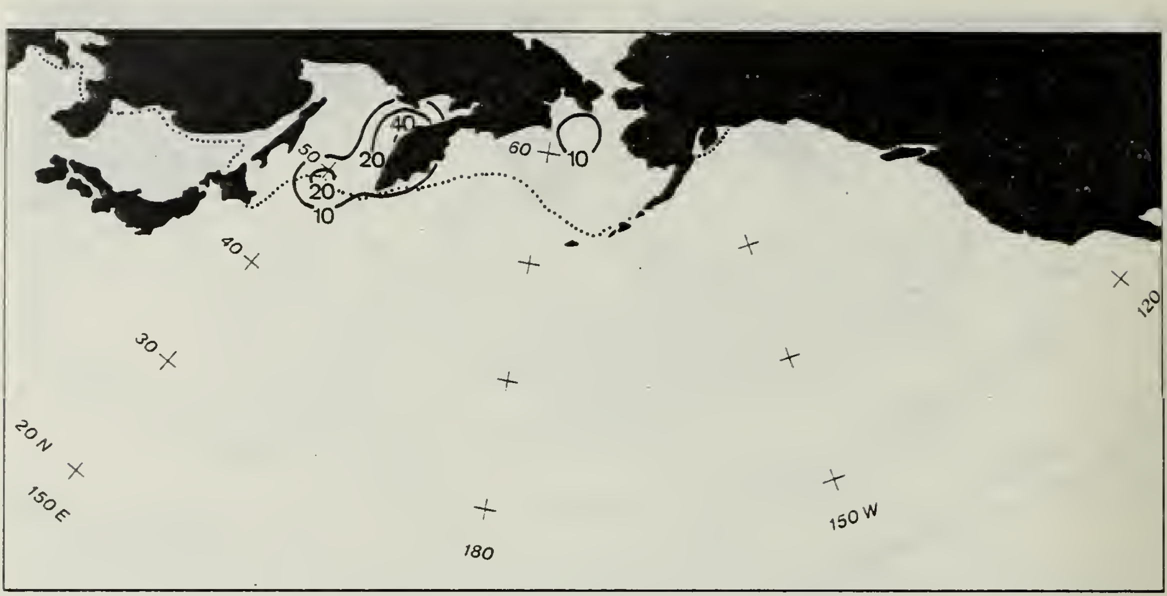

Figure 22a. January 1200 GMT frequency of visibility less than 2 km (solid lines) (%), maximum southern extent of ice coverage .1 or greater (dotted line), (U.S. Naval Weather Service Environmental Detachment, 1977).

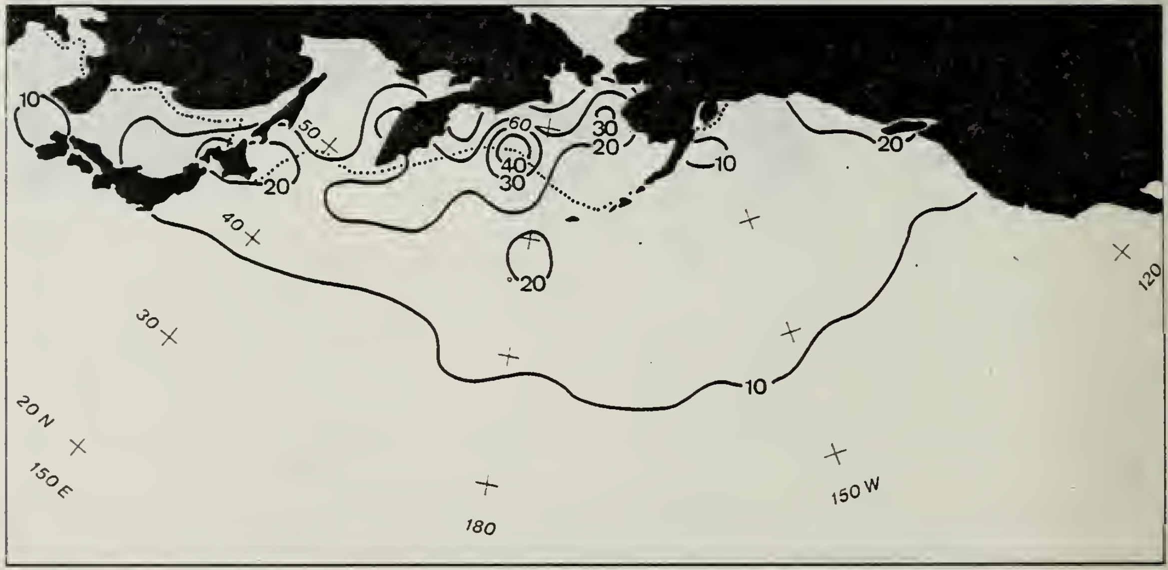

Figure 22b. January 0000 GMT frequency of visibility equal to or greater than 2 km and less than 10 km (solid lines) (%), maximum southern extent of ice coverage .1 or greater (dotted line), (U.S. Naval Weather Service Environmental Detachment, 1977).

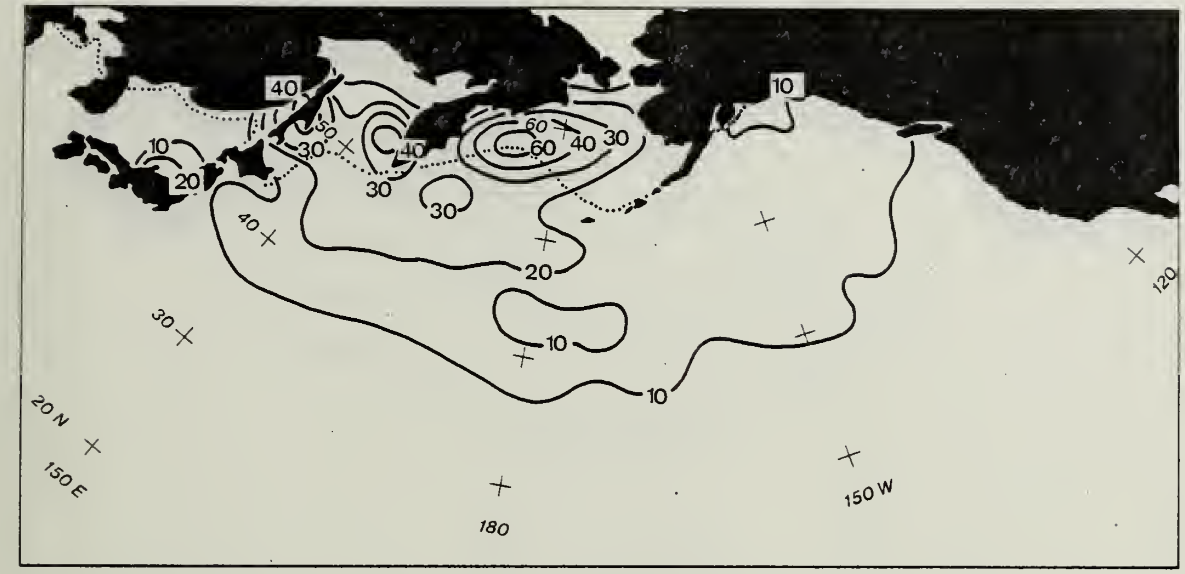

Figure 23a. January 1200 GMT frequency of visibility equal to or greater than 2 km and less than 10 km (solid lines) (%), maximum southern extent of ice coverage .1 or greater (dotted line), (U.S. Naval Weather Service Environmental Detachment, 1977).

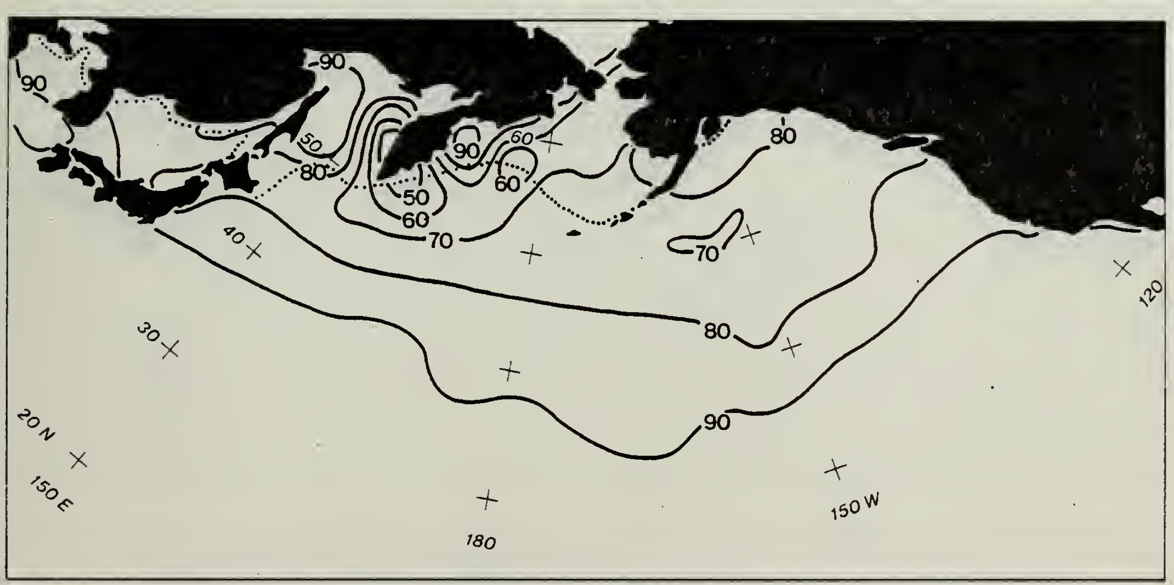

Figure 23b. January 0000 GMT frequency of visibility equal to or greater than 10 km (solid lines) (%), maximum southern extent of ice coverage .1 or greater (dotted line), (U.S. Naval Weather Service Environmental Detachment, 1977).

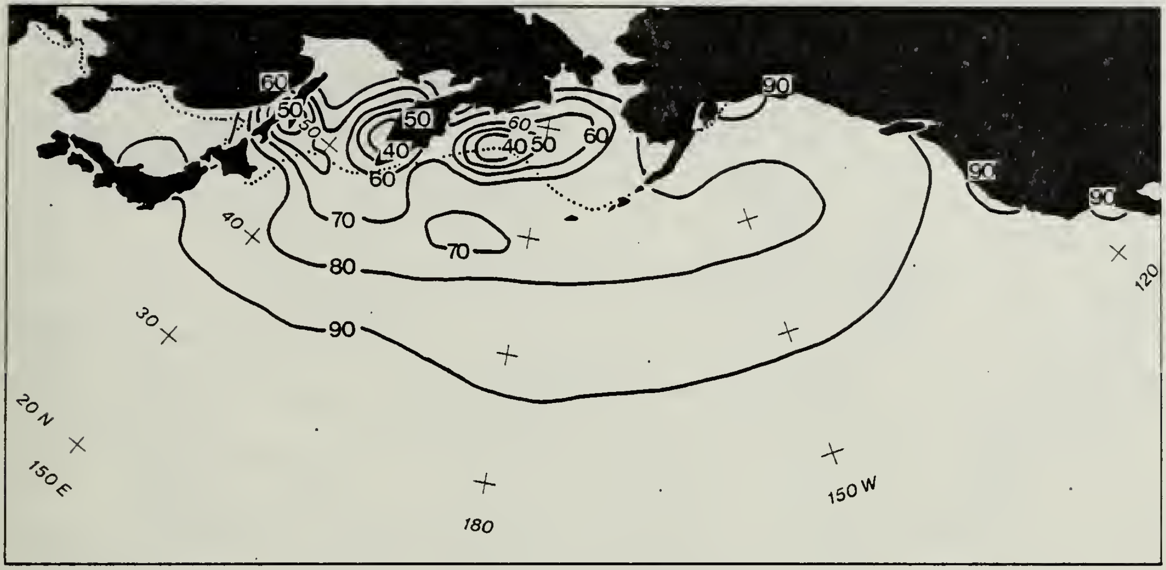

Figure 24a. January 1200 GMT frequency of visibility equal to or greater than 10 km (solid lines) (%), maximum southern extent of ice coverage .1 or greater (dotted line), (U.S. Naval Weather Service Environmental Detachment, 1977).

Figure 24b. January frequency of fog occurrence (solid lines) (%), maximum southern extent of ice coverage .1 or greater (dotted line), (U.S. Naval Weather Service Environmental Detachment, 1977).

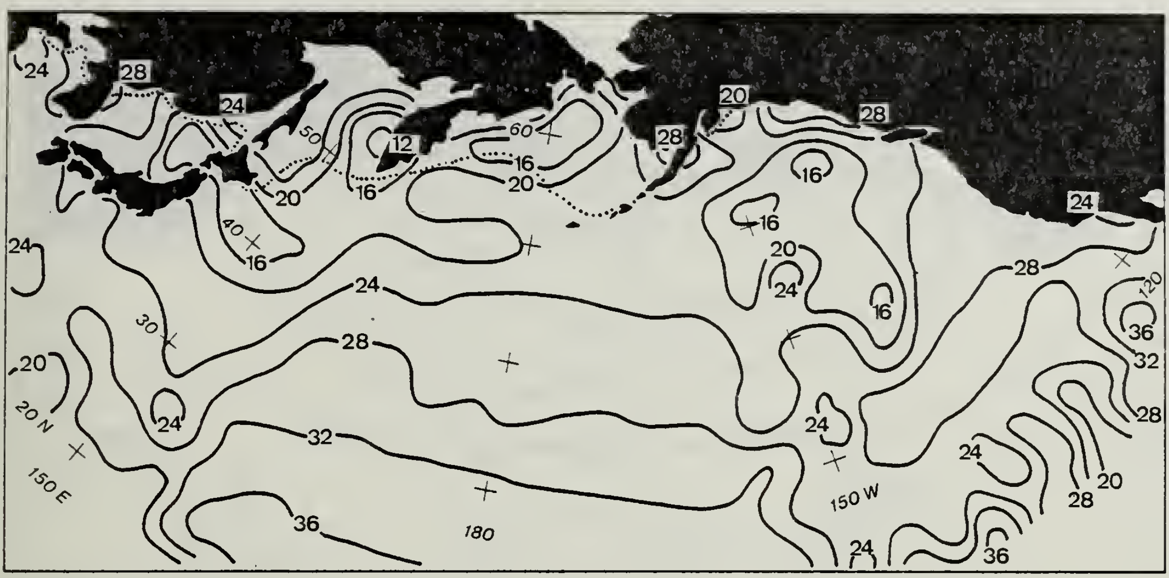

Figure 25a. January 0000 LST mean surface visibility analysis (km) (solid lines), maximum southern extent of ice coverage .1 or greater (dotted line), (U.S. Naval Weather Service Environmental Detachment, 1977).

Figure 25b. Same as 25a for 0130 LST.

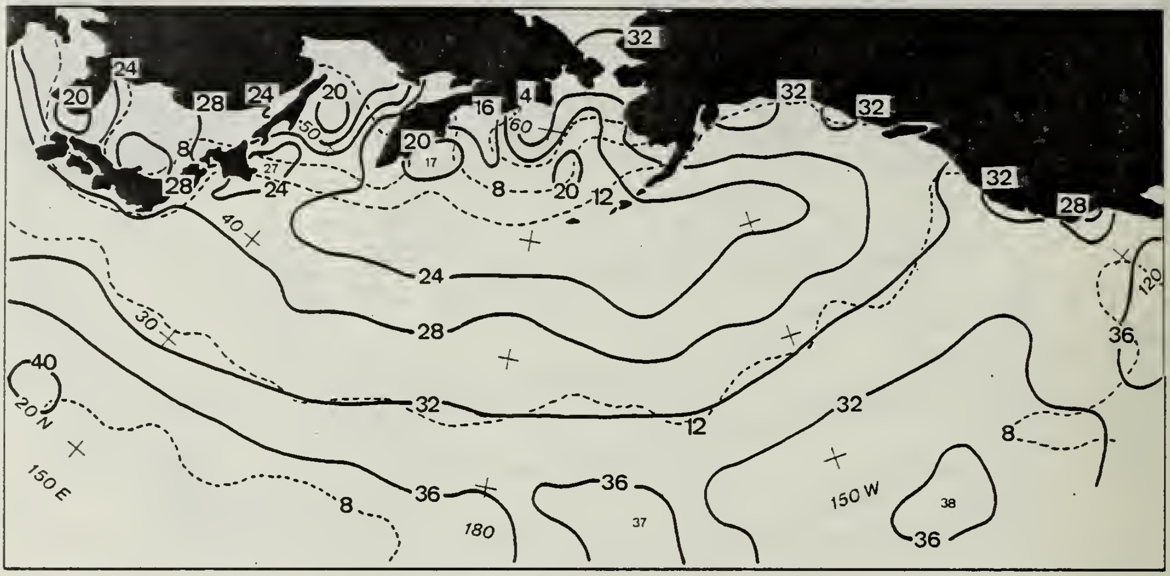

Figure 26a. April 0000 GMT mean surface visibility (km) (solid lines), standard deviations at 4 km intervals (dashed lines).

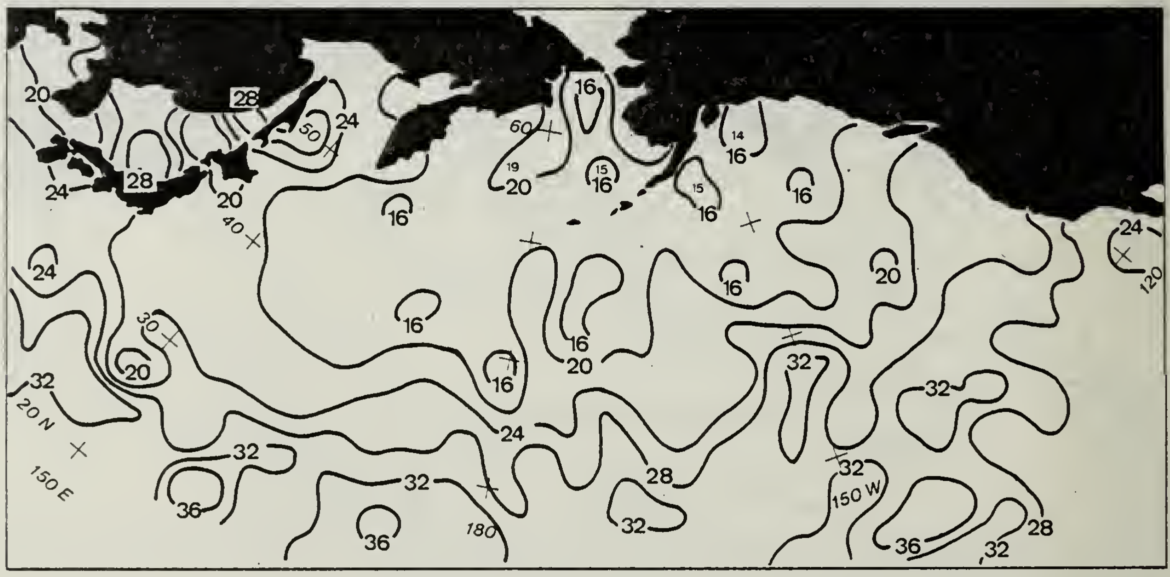

Figure 26b. April 0900 GMT mean surface visibility (km).

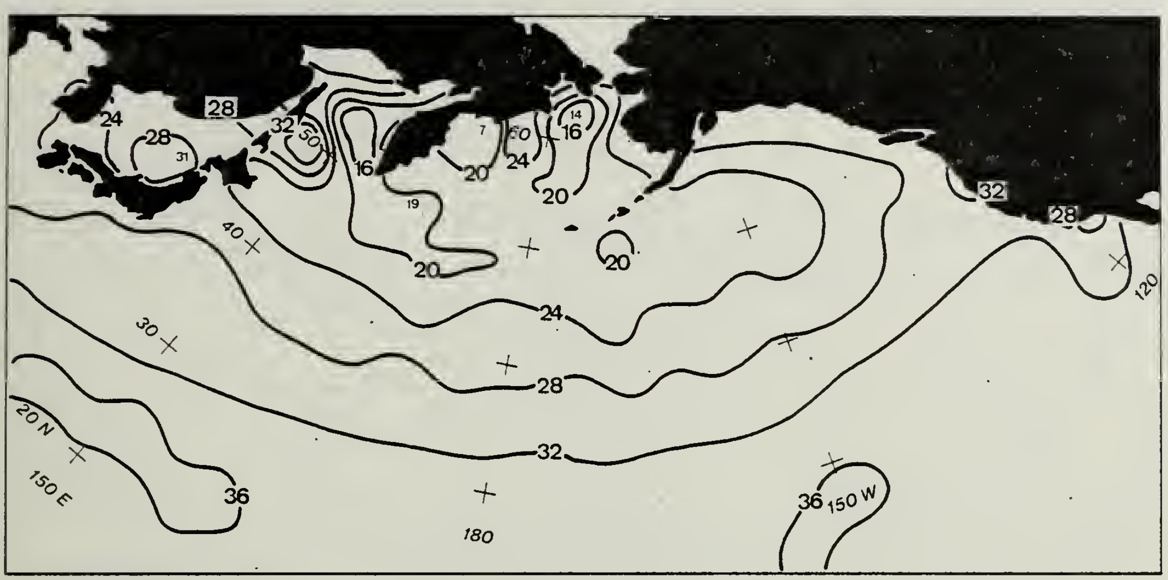

Figure 27a. April 1200 GMT mean surface visibility (km).

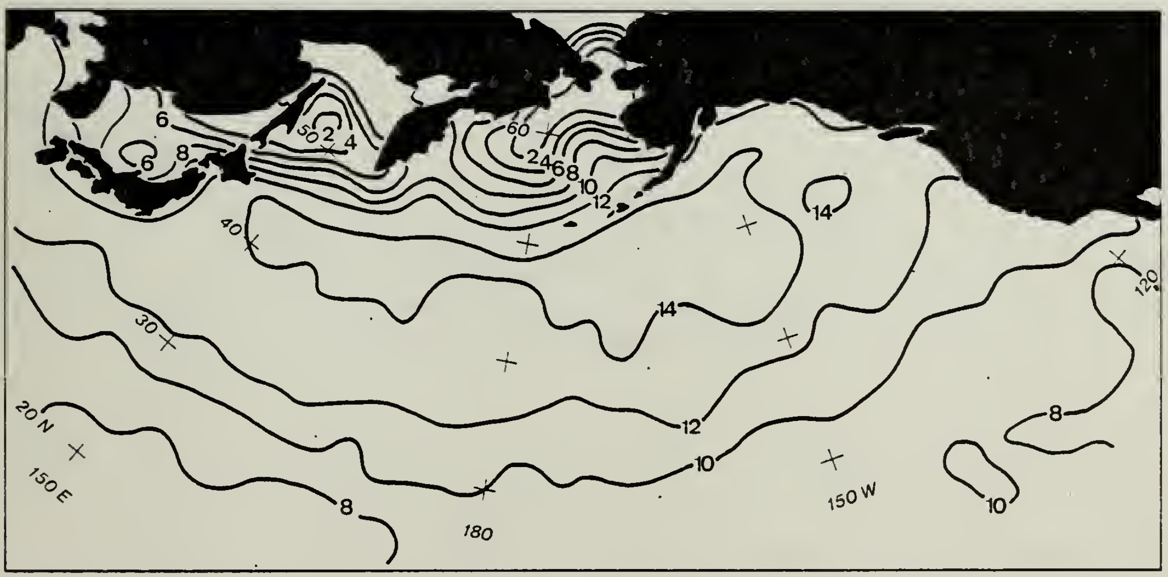

Figure 27b. April 0000 GMT standard deviations of surface visibility (km).

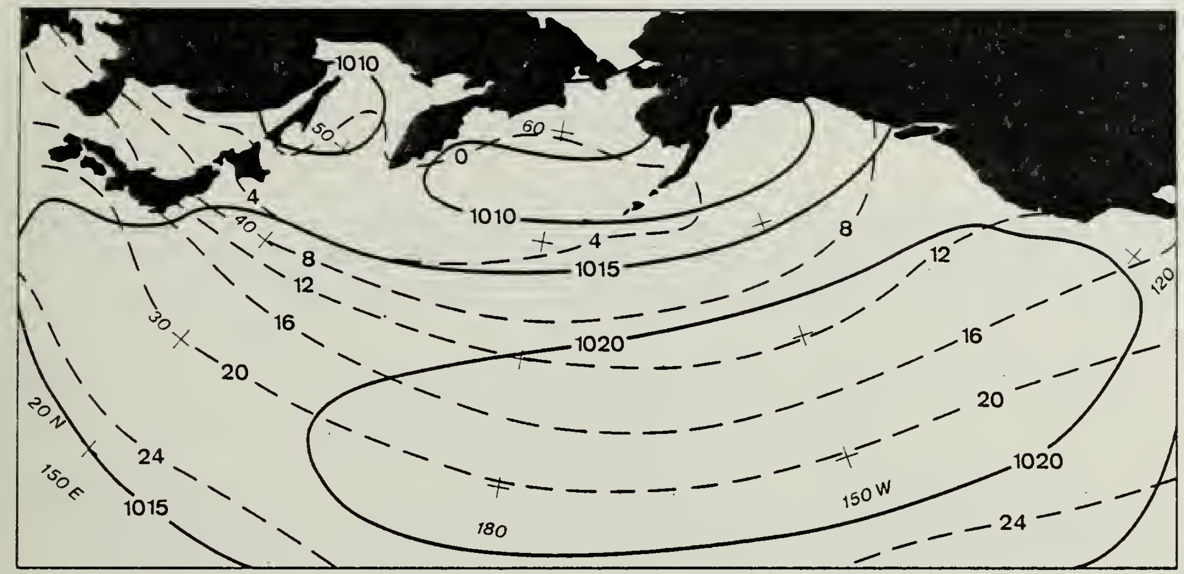

Figure 28a. April mean sea-level pressure (mb) (solid lines), mean sea-surface temperatures (°C) (dashed lines) for the North Pacific Ocean, (U.S. Naval Weather Service Environmental Detachment, 1977).

Figure 28b. April frequency of fog occurrence (%).

LIST OF REFERENCES

Aldinger, W. T., 1979: Experiments on Estimating Ocean Visibilities Using Model-Output Statistics. M.S. Thesis, Dept. of Meteorology, Naval Postgraduate School, Monterey, CA, 81 pp.

Cressman, G. P., 1959: An Operational Objective Analysis System. Mon. Wea. Rev., 87, p. 367-374.

Englebretson, R. E., 1974: A Synthesis of the Elements of Random-Ship Synoptic Reports to Derive Climatological Marine-Fog Frequencies. M.S. Thesis, Dept. of Meteorology, Naval Postgraduate School, Monterey, CA, 68 pp.

Koziara, M. C., 1980: Further Development of a Statistical Model to Specify Marine Fog Probability Using Numerically Derived Model Output Parameters. M.S. Thesis, Dept. of Meteorology, Naval Postgraduate School, Monterey, CA, 83 pp.

Nelson, T. S., 1972: Numerical-Statistical Prediction of Visibility at Sea. M.S. Thesis, Dept. of Meteorology, Naval Postgraduate School, Monterey, CA, 36 pp.

Quayle, R. G., 1974: A Climatic Comparison of Ocean Weather Stations and Transient Ship Records. Mariners Weather Log, Vol. 18, No. 5, September 1974, p. 307-311.

Renard, R. J., 1976: The Observation, Analysis, Forecasting and Climatology of Marine Fog, WMO. No. 454, The Applications of Marine Meteorology to the High Seas Coastal Zone Development. World Met. Organization, Geneva, Switzerland, 211-223.

Schramm, W. G., 1966: Analysis and Prediction of Visibility at Sea. M.S. Thesis, Dept. of Meteorology, Naval Postgraduate School, Monterey, CA, 54 pp.

Selsor, H. D., 1980: Further Experments Using a Model Output Statistics Method in Estimating Open Ocean Visibility. M.S. Thesis, Dept. of Meteorology, Naval Postgraduate School, Monterey, CA, 121 pp.

Yavorsky, P. G., and Renard, R. J., 1980: Experiments Concerning Categorical Forecasts of Open-Ocean Visibility Using Model Output Statistics. NPS Report NPS63-80-002, Dept. of Meteorology, Naval Postgraduate School, Monterey, CA, 87 pp.

Wheeler, S. E., and Leipper, D. F., 1974: Marine Fog Impact on Naval Operations. NPS Report 58Wh 74091, Dept. of Meteorology, Naval Postgraduate School, Monterey, CA, 118 pp.

U.S.Naval Weather Service Environmental Detachment, 1974: Northeast Pacific Environmental Scenario, U.S. Naval Weather Service Environmental Detachment, Asheville, NC, 263 pp.

______, 1977: U.S. Navy Marine Climatic Atlas of the World, Vol. II, NAVAIR 50-1C-529, U.S. Naval Weather Service Environmental Detachment, Asheville, NC, 388 pp.

Willms, G. P., 1975: A Climatology of Marine-Fog Frequencies for the North Pacific Ocean Summer Fog Season. M.S. Thesis, Dept. of Meteorology, Naval Postgraduate School, Monterey, CA, 59 pp.

World Meteorological Organization, 1979: Meteorological Surface Observations. WMO No. 49, Technical Regulations. World Met. Organization, Geneva, Switzerland, A.1.2-6 - A.1.2-7.

BIBLIOGRAPHY

Barker, E. H., 1975: A Maritime Boundary Layer Model for the Prediction of Fog, Tech. Paper No. 4-75, Environmental Prediction Research Facility, Naval Postgraduate School, Monterey, CA, 51 pp.

_____, 1980: Analysis and Initialization Procedure for the Navy Operational Global Atmospheric Prediction System. Naval Environmental Prediction Research Facility, Monterey, CA, 40 p.

Gandin, L. S., 1963: Objective Analysis of Meteorological Fields, translated from Russian by Israel Program for Scientific Translations, 1965, 242 p. [NTIS No. TT 65-50007].

Grisham, P. O., 1971: An Investigation of Marine Fog Formation and Occurrence over the North Pacific Ocean Area. Research Paper, Dept. of Meteorology, Naval Postgraduate School, Monterey, CA, 35 pp.

Haltiner, G. J. and R. T. Williams, 1980: Numerical Prediction and Dynamic Meteorology, John Wiley and Sons, NY, Toronto, 477 pp.

Jarvinen, B., 1974: Objective Analysis of Sea-Surface Temperatures Using Marine Observations. Mariners Weather Log, Vol. 18, No. 5, September 1974, p. 304-306.

Middleton, W.E.K., 1951: Visibility in Meteorology. Compendium of Meteorology, Boston, Amer. Meteor. Soc., 1315 pp.

_____, 1952: Vision Through the Atmosphere. Toronto, University of Toronto Press, 246 pp.

Muromtsev, A. M., 1958: The Principal Hydrological Features of the Pacific Ocean. Translated from Russian by Israel Program for Scientific Translations, 1963, 417 pp. [NTIS No. TT 63-11065].

Petterssen, S., 1938: On the Causes and Forecasting of the California Fog. Bull. Amer. Meteor. Soc., 19, 49-55.

Roll, H. U., 1965: <u>Physics of the Marine Atmosphere</u>. New York, Academic Press, 426 pp.

Taylor, G. L., 1917: The Formation of Fog and Mist. <u>Quart. J. Roy. Meteor. Soc</u>., <u>43</u>, 241-268.

INITIAL DISTRIBUTION LIST

		No. Copies
1.	Defense Technical Information Center Cameron Station Alexandria, Virginia 22314	2
2.	Library, Code 0142 Naval Postgraduate School Monterey, California 93940	2
3.	Air Weather Service Technical Library Scott AFB, Illinois 62225	1
4.	Dr. Robert J. Renard, Code 63Rd Department of Meteorology Naval Postgraduate School Monterey, California 93940	10
5.	Captain Philip G. Yavorsky 903 Canada Goose Drive Suisun City, California 94585	1
6.	Captain Thomas N. Talbot Route #1 Winchester, New Hampshire 03470	4
7.	Commanding Officer Fleet Numerical Oceanography Center Monterey, California 93940	1
8.	Commanding Officer Naval Environmental Prediction Research Facility Monterey, California 93940	1
9.	Dr. Andrzej Goroch Naval Environmental Prediction Research Facility Monterey, California 93940	1
10.	Meteorology Reference Center, Code 63 Department of Meteorology Naval Postgraduate School Monterey, California 93940	1

11. Captain Brian Van Orman 2
AFIT/CIRF
Wright/Patterson AFB, Ohio 45433

12. Mr. Leo Clarke 1
Fleet Numerical Oceanography Center
Monterey, California 93940

13. Naval Air Systems Command 1
Attn: Cdr K. Van Sickle (AIR-370)
Washington, DC 20360

14. Chairman, Department of Oceanography, Code 68 1
Naval Postgraduate School
Monterey, California 93940

15. Officer in Charge 1
Naval Oceanography Command Detachment
Federal Building
Asheville, North Carolina 28801

16. Mr. William Rogers 1
CALSPAN Advanced Technology Center
P. O. Box 400
Buffalo, New York 14225

17. Dr. Dale Leipper, Code 68Lr 1
Department of Oceanography
Naval Postgraduate School
Monterey, California 93940

18. Dr. Glenn H. Jung, Code 68Jg 1
Department of Oceanography
Naval Postgraduate School
Monterey, California 93940

19. Director 1
Naval Oceanography Division
Naval Observatory
34th and Massachusetts Avenue NW
Washington, DC 20390

20. Commander 1
Naval Oceanography Command
NSTL Station
Bay St. Louis, Mississippi 39522

21. Commanding Officer 1
Naval Oceanographic Office
NSTL Station
Bay St. Louis, Mississippi 39522

22. Commanding Officer 1
Naval Ocean Research and Development Activity
NSTL Station
Bay St. Louis, Mississippi 39522

23. Chairman, Oceanography Department 1
U. S. Naval Academy
Annapolis, Maryland 21402

24. Chief of Naval Research 1
800 N. Quincy Street
Arlington, Virginia 22217

25. Chief of Naval Research (Code 480) 1
Naval Ocean Research and Development Activity
NSTL Station
Bay St. Louis, Mississippi 39522

26. Commander 1
Air Weather Service
Scott Air Force Base, Illinois 62225

27. Commanding Officer 1
Air Force Global Weather Central
Offutt Air Force Base, Nebraska 68113

28. Chief, Ocean Services Division 1
National Oceanic and Atmospheric
  Administration
8060 Thirteenth Street
Silver Springs, Maryland 20910

193702
Thesis
T133 Talbot
c.1 Development of a prototype North Pacific Ocean surface visibility climatory stratified by observation times.